Inorganic Chemistry

pubs.acs.org/IC

Article

Open-Ended Metallodithiolene Complexes with the 1,2,4,5-Tetrakis(diphenylphosphino)benzene Ligand: Modular Building Elements for the Synthesis of Multimetal Complexes

Satyendra Kumar,* Malathy Selvachandran, Kuppuswamy Arumugam, Mohamed C. Shaw, Che Wu, Michael Maurer, Xiaodong Zhang, Stephen Sproules, Joel T. Mague, and James P. Donahue*

Cite This: *Inorg. Chem.* 2021, 60, 13177−13192

Read Online

ACCESS | Metrics & More | Article Recommendations | Supporting Information

ABSTRACT: Open-ended, singly metalated dithiolene complexes with 1,2,4,5-tetrakis(diphenylphosphino)benzene (tpbz) are prepared either by ligand transfer to $[Cl_2M(tpbz)]$ from $(R_2C_2S_2)SnR'_2$ (R = CN, R′ = Me; R = Me, R′ = ^{n}Bu) or by a direct reaction between tpbz and $[M(S_2C_2R_2)_2]$ (M = Ni, Pd, Pt; R = Ph, *p*-anisyl) in a 1:1 ratio. The formation of dimetallic $[(R_2C_2S_2)M(tpbz)M(S_2C_2R_2)]$ attends these syntheses in modest amounts, but the open-ended compounds are readily separated by silica chromatography. As affirmed by X-ray crystallographic characterization of numerous members of the set, the $[(R_2C_2S_2)M(tpbz)]$ compounds show dithiolene ligands in their fully reduced ene-1,2-dithiolate form conjoined with divalent Group 10 ions. Minor amounts of octahedral $[(Ph_2C_2S_2)_2Pt^{IV}(tpbz)]$, a presumed intermediate, are isolated from the preparation of $[(Ph_2C_2S_2)Pt^{II}(tpbz)]$. Heterodimetallic $[(Ph_2C_2S_2)Pt(tpbz)Ni(S_2C_2Me_2)]$ is prepared from $[(Ph_2C_2S_2)Pt^{II}(tpbz)]$; its cyclic voltammogram, upon anodic scanning, shows two pairs of closely spaced, but resolved, 1e$^-$ oxidations corresponding first to $[R_2C_2S_2^{2-}] - 1e^- \rightarrow [R_2C_2S^{\bullet}S^-]$ and then to $[R_2C_2S^{\bullet}S^-] - 1e^- \rightarrow [R_2(C{=}S)_2]$. The open diphosphine of $[(R_2C_2S_2)M(tpbz)]$ can be oxidized to afford open-ended $[(R_2C_2S_2)M(tpbzE_2)]$ (E = O, S). Synthesis of the octahedral $[(dppbO_2)_3Ni][I_3]_2$ [$dppbO_2$ = 1,2-bis(diphenylphosphoryl)benzene] suggests that the steric profile of $[(R_2C_2S_2)M(tpbzE_2)]$ is moderated enough that three could be accommodated as ligands around a metal ion.

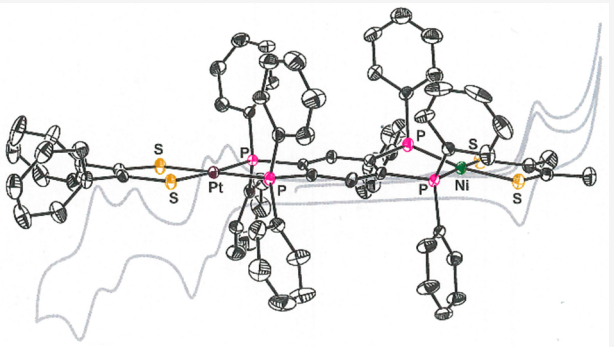

INTRODUCTION

In recent work,[1,2] we have reported the synthesis, structures, and properties of a set of dimetallic compounds of the type $[(R_2C_2S_2)M(tpbz)M(S_2C_2R_2)]$ [tpbz = 1,2,4,5-tetrakis-(diphenylphosphino)benzene], where R may be CN, Me, Ph, or *p*-anisyl and, independent of R, M may be varied as Ni^{2+}, Pd^{2+}, or Pt^{2+}. The dithiolene end groups can be concurrently oxidized to radical monoanions (**a** → **b**, Scheme 1), thus providing $[(R_2C_2S^-S^{\bullet})M(tpbz)M(S^-S^{\bullet}C_2R_2)]^{2+}$ dications, which weakly couple to provide nearly isoenergetic S = 1 and 0 states in equilibrium. Electron paramagnetic resonance (EPR) spectroscopy is effective in characterizing subtle differences among the $[(R_2C_2S_2)M(tpbz)M(S_2C_2R_2)]^{2+}$ complexes as M and R are varied. For example, simulations of the EPR spectra of $[((MeO\text{-}p\text{-}C_6H_4)_2C_2S_2)M(tpbz)M(S_2C_2(C_6H_4\text{-}p\text{-}OMe)_2)]^{2+}$, where M = Ni^{2+} or Pd^{2+}, yield D = -18×10^{-4} cm^{-1} and -15×10^{-4} cm^{-1}, respectively, with the former value indicative of a slightly shorter distance between the spin barycenters because of greater spin delocalization onto the metal from the dithiolene radicals.

The conditions for the syntheses of $[(R_2C_2S_2)M(tpbz)M(S_2C_2R_2)]$ that we reported were devised to promote formation of the dimetallic species. However, when the tpbz ligand is introduced to a source of the Group 10 metal bis(dithiolene) complex in an amount that is greater than the 1:2 ratio that is optimal for $[(R_2C_2S_2)M(tpbz)M(S_2C_2R_2)]$, we

Scheme 1. Redox Levels Available to a Dithiolene Ligand When Bound to a Transition Metal

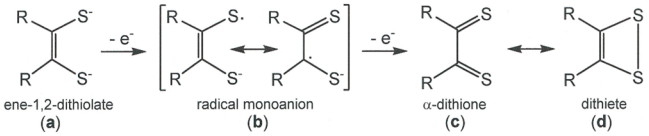

Received: May 25, 2021
Published: August 9, 2021

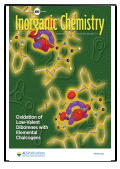

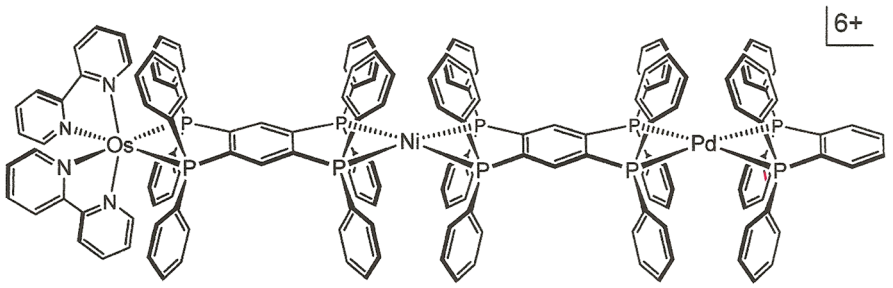

Figure 1. A previously reported[3] tpbz-linked heterotrimetallic complex designed to support gated photoinduced electron transfer.

Scheme 2. Syntheses of Open-Ended $[(R_2C_2S_2)M(tpbz)]$ (M = Ni^{2+}, Pd^{2+}, Pt^{2+}; R = Me, Ph, CH_3O-*p*-C_6H_4, CN) Compounds

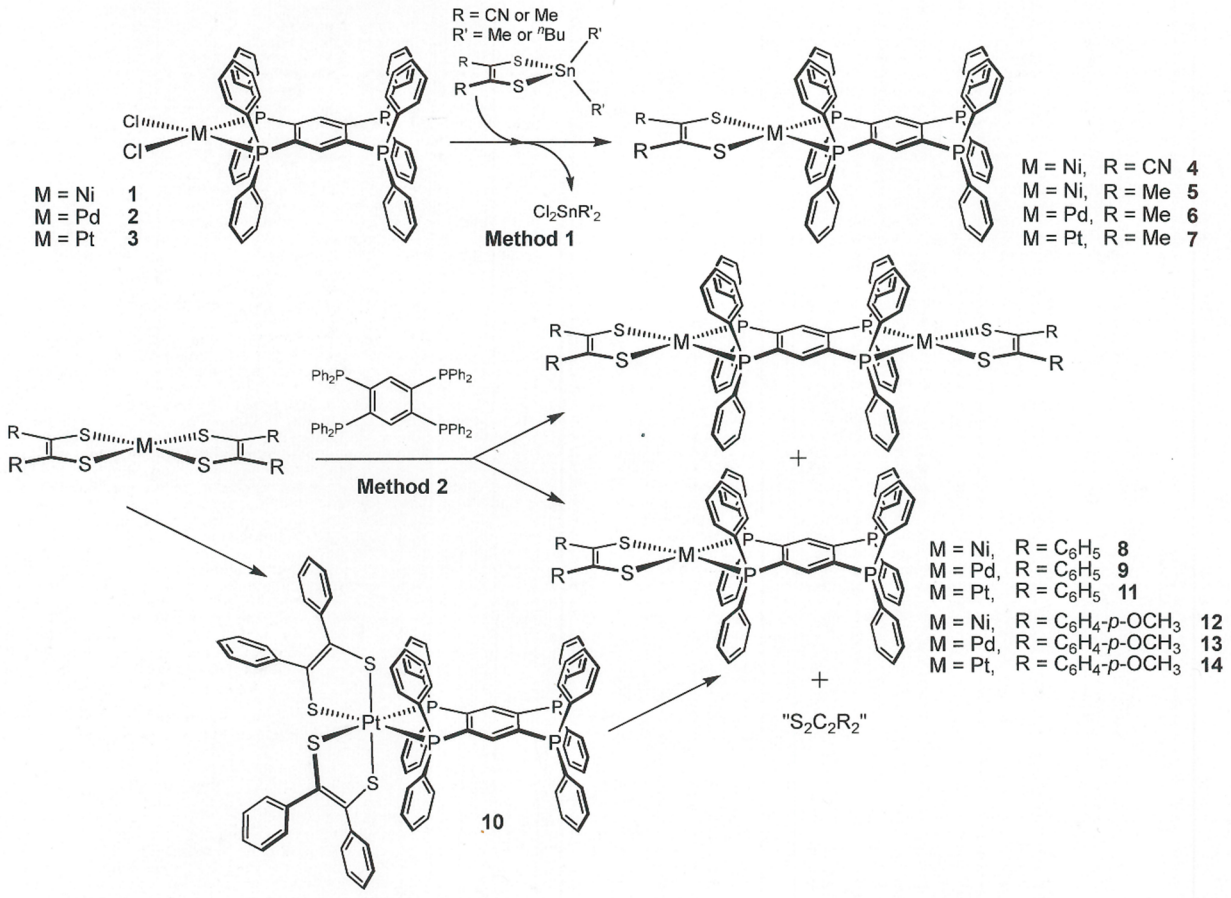

have noted that "open-ended" tpbz compounds can be isolated in which only one of the two chelating sites is occupied. Although the centrosymmetic dimetal compounds still form, they are readily separated from the open-ended compounds because of their lowered solubility and slower movement on silica columns. These open-ended monometallic compounds still possess the air and moisture stability enjoyed by the free tpbz ligand itself, thus making them easily accessible in quantities that can be deployed for further synthetic ends. In every sense of the term, these open-ended complexes are themselves ligands, or "modules," for the systematic creation of higher-order assemblies incorporating other metal ions with the capacity for a specific function. Zahavy and Fox, for example, described trimetallic $[(bpy)_2Os(tpbz)Ni(tpbz)Pd(dppb)]^{6+}$ (Figure 1), the synthesis of which proceeded through open-ended $[(bpy)_2Os(tpbz)]^{2+}$, as a photoinduced Os → Pd electron transfer device with gating controlled by the redox state at Ni.[3]

In general terms, modular chemical synthesis may be described as the preparation of materials or discrete compounds from two or more sets of parts such that (1) an array of products whose number is the product of the numbers of the members of the constituents sets can be obtained, (2) a common synthetic methodology can be executed for the synthesis of all products, and (3) desirable properties of the resulting materials, such as the redox potential or acidity, may be varied with a predictable effect. Arguably, the most prominent example of modular synthesis is the synthesis of metal−organic frameworks, wherein "nodes" defined by transition-metal ions with varying coordination environment constraints are joined by any of an array of chemical linkers to produce open spacings or channels.[4] A rather different example from Lu and co-workers is the installment, via a two-step

https://doi.org/10.1021/acs.inorgchem.1c01573
Inorg. Chem. 2021, 60, 13177−13192

Scheme 3. Syntheses of Pt−Ni Heterodimetallic 15 and Oxidized Open-Ended Compounds 16−18

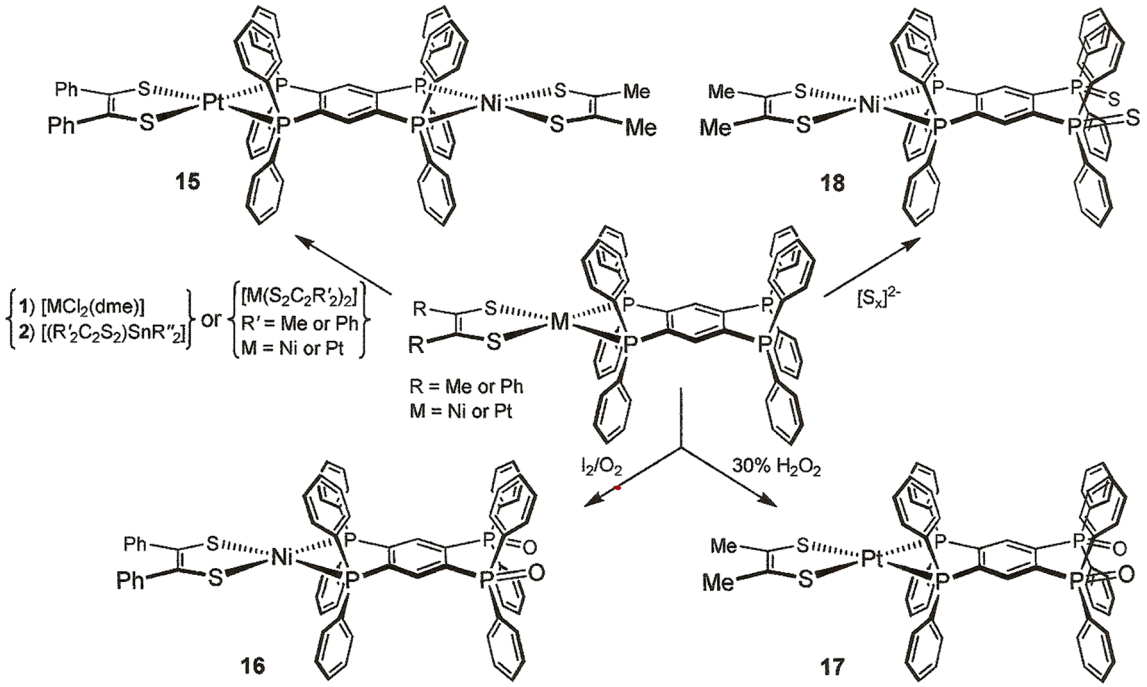

metalation protocol, of heterodimetallic units within a variety of tripodal ligands whose arms feature three-atom bridges.[5] An obvious advantage of modular synthesis is the efficiency it can provide toward identifying an optimal candidate for a particular application.

In this report, we provide an account of the synthesis and characterization of the open-ended $[(R_2C_2S_2)M(tpbz)]$ compounds that are summarized pictorially in Scheme 2. A particular emphasis is placed on the solid-state molecular structures and on ^{31}P NMR spectroscopy as a convenient and definitive handle for characterization of these compounds. Following their isolation, postsynthetic modification of $[(R_2C_2S_2)M(tpbz)]$ by oxidation of the noncoordinating P sites to the corresponding phosphine oxide or sulfide is possible and provides a further dimension of variability for this metallodithiolene "module" (Scheme 3). Using isolated $[(R_2C_2S_2)M(tpbz)]$, asymmetric heterodimetallic complexes of the form $[(R_2C_2S_2)M(tpbz)M'(S_2C_2R'_2)]$ ($M' \neq M$; $R \neq R'$) are readily prepared that are not accessible by the method originally disclosed for $[(R_2C_2S_2)M(tpbz)M(S_2C_2R_2)]$.

SYNTHESES

General Considerations. Literature methods were implemented for the syntheses of $[Cl_2Ni(dme)]$[6] (dme = 1,2-dimethoxyethane), $[Cl_2M(NCCH_3)_2]$ (M = Pd^{2+}, Pt^{2+}),[7] $[(R_2C_2S_2)_2M]$ (R = Me, Ph, *p*-anisyl; M = Ni^{2+}, Pd^{2+}, Pt^{2+}),[8] $[((NC)_2C_2S_2)SnMe_2]$, $[(Me_2C_2S_2)Sn(^nBu)_2]$, the tpbz ligand,[9] and 1,2-bis(diphenylphosphino)benzene dioxide ($dppbO_2$).[10] All other reagents were purchased from commercial sources and used as received. Solvents were either dried with a system of drying columns from the Glass Contour Company [dichloromethane (CH_2Cl_2), *n*-pentane, hexanes, diethyl ether (Et_2O), tetrahydrofuran (THF), benzene (C_6H_6), and toluene] or freshly distilled according to standard procedures [methanol (MeOH), acetonitrile (CH_3CN), and 1,2-dichloroethane].[11] All reactions described below were conducted under an atmosphere of N_2, while silica columns were run in the open air using 60−230 μm silica (Dynamic Adsorbents). Dithiolene ligand abbreviations used throughout the text are as follows: mdt = $[Me_2C_2S_2]^{2-}$ = 1,2-dimethyl-1,2-dithiolate(2−); mnt = $[(NC)_2C_2S_2]^{2-}$ = maleonitriledithiolate(2−); pdt = $[Ph_2C_2S_2]^{2-}$ = 1,2-diphenyl-1,2-dithiolate(2−); adt = $[(MeO\text{-}p\text{-}C_6H_4)_2C_2S_2]^{2-}$ = 1,2-di-*p*-anisyl-1,2-dithiolate(2−).

Physical Methods. All ^1H and ^{31}P NMR spectra were recorded at 25 °C with a Bruker Avance spectrometer operating at 300.13 and 121.49 MHz for the ^1H and ^{31}P nuclei, respectively. The ^1H NMR spectra were referenced to the solvent signal, while an external aqueous phosphoric acid (H_3PO_4) solution was employed as the reference for all ^{31}P NMR spectra. Mass spectra (positive-ion electrospray ionization, ESI^+) were obtained with a Bruker micrOTOF II mass spectrometer. The X-band EPR spectrum was recorded on a Bruker ELEXSYS E500 spectrometer. Electrochemical measurements were made with a CHI620C electroanalyzer workstation using a Ag/AgCl reference electrode, a glassy carbon or Pt disk working electrode, a Pt wire auxiliary electrode, and a $[^nBu_4N][PF_6]$ supporting electrolyte. Under these conditions, the Cp_2Fe^+/Cp_2Fe (Fc^+/Fc) couple consistently occurred at +0.436 mV in CH_2Cl_2. Elemental analyses were performed by Midwest Microlab, LLC (Indianapolis, IN), Galbraith Laboratories, Inc. (Knoxville, TN), or Kolbe Microanalytical Laboratory (Oberhausen, Germany). Procedural details regarding crystal growth, X-ray diffraction data collection, data processing, and structure solution and refinement are available in the Supporting Information. Unit cell data and selected refinement statistics are presented in Table 1.

$[Cl_2Ni(tpbz)]$ (1). A 50 mL Schlenk flask charged with $[Cl_2Ni(dme)]$ (0.022 g, 0.10 mmol), tpbz (0.081 g, 0.10 mmol), and CH_2Cl_2 (15 mL) was stirred for 1 h at ambient temperature, during which time a dark-red color developed. The reaction mixture was filtered to remove undissolved materials, and the filtrate was taken to dryness under reduced pressure to afford an orange-red solid residual that was suitable for use without further purification. Yield: 0.075 g, 0.079 mmol, 79%. ^1H NMR (CD_2Cl_2): δ 9.63−9.51 (m, 11H, aromatic C−*H*), 9.34−9.15 (m, 14H, aromatic C−*H*), 8.98−8.78 (m, 17H, aromatic C−*H*). $^{31}P\{^1H\}$ NMR (CD_2Cl_2): δ 49.9 (s), −14.1 (s).

$[Cl_2Pd(tpbz)]$ (2). A 50 mL Schlenk flask was charged with $[PdCl_2(CH_3CN)_2]$ (0.026 g, 0.10 mmol), tpbz (0.081 g, 0.10 mmol), and a 1:1 mixture of CH_2Cl_2/CH_3CN (20 mL). The resulting mixture was stirred at ambient temperature for 12 h in the dark, during which time a light-yellow solution developed. The solvent was removed under reduced pressure, and the residual light-yellow solid was

https://doi.org/10.1021/acs.inorgchem.1c01573
Inorg. Chem. 2021, 60, 13177−13192

Table 1. Unit Cell and Refinement Data for Compounds Characterized by X-ray Diffraction

compound	[Cl_2Ni(tpbz)]	[(mnt)Ni(tpbz)]	[(mdt)Ni(tpbz)]	[(mdt)Pt(tpbz)]
compound no.	**1**	**4**	**5**	**7**
cocryst solvent	Et_2O	$2CHCl_3$	$2CH_2Cl_2$	$2CH_2Cl_2$
formula	$C_{58}H_{52}Cl_2NiOP_4$	$C_{60}H_{44}Cl_6N_2NiP_4S_2$	$C_{60}H_{52}Cl_4NiP_4S_2$	$C_{60}H_{52}Cl_4P_4PtS_2$
fw, g mol^{-1}	1018.49	1252.38	1161.52	1297.91
temperature, K	100	100	100	100
wavelength, Å	0.71073	0.71073	0.71073	0.71073
2θ range, deg	2.34−55.70	4.22−56.74	3.24−60.44	3.22−56.56
cryst syst	orthorhombic	orthorhombic	monoclinic	monoclinic
space group	$Pna2_1$	$P2_12_12_1$	$C2/c$	$C2/c$
a, Å	34.703(3)	13.510(3)	21.223(2)	21.157(5)
b, Å	9.2939(9)	16.403(3)	15.7180(18)	15.836(4)
c, Å	15.5064(14)	25.380(5)	16.7123(18)	16.576(4)
α, deg	90	90	90	90
β, deg	90	90	100.039(2)	99.604(4)
γ, deg	90	90	90	90
volume (Å^3), Z	5001.2(8), 4	5624.2(19), 4	5489.6(11), 4	5476(2), 4
density, g cm^{-3}	1.353	1.479	1.405	1.574
μ, mm^{-1}	0.664	0.860	0.780	2.991
color, habit	orange plate	orange block	brwn-grn column	yellow plate
limiting indices h	$-44 \le h \le 45$	$-17 \le h \le 18$	$-29 \le h \le 29$	$-28 \le h \le 27$
limiting indices k	$-12 \le k \le 12$	$-21 \le k \le 21$	$-22 \le k \le 22$	$-20 \le k \le 20$
limiting indices l	$-20 \le l \le 19$	$-33 \le l \le 33$	$-23 \le l \le 23$	$-21 \le l \le 21$
reflns collected	40918	100119	52873	24025
indep data, param[a]	11569, 597	14060, 676	7799, 322	6526, 322
GOF[b]	1.090	1.048	1.105	1.035
R1,[c,d] wR2[d,e]	0.0574, 0.1259	0.0413, 0.1087	0.0450, 0.1434	0.0308, 0.0750
R1,[c,f] wR2[e,f]	0.0725, 0.1327	0.0481, 0.1141	0.0590, 0.1468	0.0360, 0.0776
compound	[(pdt)Ni(tpbz)]	[(pdt)Pd(tpbz)]	[(pdt)Pt(tpbz)]	[$(pdt)_2$Pt(tpbz)]
compound no.	**8**	**9**	**11**	**10**
cocryst solvent	none	none	none	$2(ClCH_2CH_2Cl)$
formula	$C_{68}H_{52}NiP_4S_2$	$C_{68}H_{52}P_4PdS_2$	$C_{68}H_{52}P_4PtS_2$	$C_{86}H_{70}Cl_4P_4PtS_4$
fw, g mol^{-1}	1115.80	1163.49	1252.18	1692.43
temperature, K	150	100	100	100
wavelength, Å	1.54178	0.71073	0.71073	0.71073
2θ range, deg	6.84−148.77	3.14−58.44	3.14−57.39	3.03−59.72
cryst syst	monoclinic	monoclinic	monoclinic	triclinic
space group	$C2/c$	$C2/c$	$C2/c$	$P\bar{1}$
a, Å	21.9519(4)	21.7574(15)	21.7804(15)	13.9324(12)
b, Å	16.7831(3)	16.9716(12)	16.9661(12)	14.0989(12)
c, Å	16.4070(3)	16.2670(11)	16.2774(12)	21.2092(18)
α, deg	90	90	90	89.716(1)
β, deg	112.864(1)	112.666(1)	112.727(1)	84.452(1)
γ, deg	90	90	90	72.605(1)
volume (Å^3), Z	5569.75(18), 4	5542.8(7), 4	5547.9(7), 4	3955.7(6), 2
density, g cm^{-3}	1.331	1.394	1.499	1.421
μ, mm^{-1}	2.612	0.569	2.763	2.139
color, habit	yellow block	pale-orange column	yellow column	dark-blue block
limiting indices h	$-27 \le h \le 27$	$-29 \le h \le 28$	$-29 \le h \le 28$	$-19 \le h \le 19$
limiting indices k	$-20 \le k \le 20$	$-23 \le k \le 23$	$-22 \le k \le 22$	$-19 \le k \le 19$
limiting indices l	$-20 \le l \le 20$	$-22 \le l \le 22$	$-21 \le l \le 21$	$-29 \le l \le 29$
reflns collected	35518	26293	26168	77174
indep data, param[a]	5650, 339	7084, 339	7003, 339	21625, 909
GOF[b]	1.063	1.074	1.006	1.071
R1,[c,d] wR2[d,e]	0.0340, 0.0918	0.0408, 0.1122	0.0362, 0.0836	0.0379, 0.1019
R1,[c,f] wR2[e,f]	0.0376, 0.0952	0.0558, 0.1179	0.0487, 0.0870	0.0433, 0.1044

[a]Independent data collected and parameters refined. [b]GOF = $\{\sum[w(F_o^2 - F_c^2)^2]/(n-p)\}^{1/2}$, where n = number of reflections and p is the total number of parameters refined. [c]R1 = $\sum||F_o| - |F_c||/\sum|F_o|$. [d]$R$ indices for data cut off at $I > 2\sigma(I)$. [e]wR2 = $\{\sum[w(F_o^2 - F_c^2)^2]/\sum[w(F_o^2)^2]\}^{1/2}$; $w = 1/[\sigma^2(F_o^2) + (xP)^2 + yP]$, where $P = [2F_c^2 + \mathrm{Max}(F_o^2,0)]/3$. [f]$R$ indices for all data.

washed with Et_2O (2 × 5 mL) and dried in vacuo. This compound shows only limited solubility in common organic solvents. Yield: 0.084 g, 0.085 mmol, 85%. ^{1}H NMR (DMSO-d_6): δ 7.63−7.52 (m, 14H, aromatic C−*H*), 7.35−7.16 (m, 14H aromatic C−*H*), 6.94−

https://doi.org/10.1021/acs.inorgchem.1c01573
Inorg. Chem. 2021, 60, 13177−13192

6.79 (m, 14H, aromatic C−*H*). $^{31}P\{^1H\}$ NMR (DMSO-d_6): δ 49.5 (s), −14.4 (s).

[Cl_2Pt(tpbz)] (3). The same procedure and scale as those described for the synthesis of **2** were implemented using [$PtCl_2(CH_3CN)_2$], which yielded **3** as a white solid. Yield: 0.083 g, 0.077 mmol, 77%. ^1H NMR (DMSO-d_6): δ 7.81−7.74 (m, 12H, aromatic C−*H*), 7.64−7.56 (m, 22H, aromatic C−*H*), 7.30−7.22 (m, 8H, aromatic C−*H*). $^{31}P\{^1H\}$ NMR (DMSO-d_6): δ 39.1 (s), −14.1 (s).

[(mnt)Ni(tpbz)] (4). Under an atmosphere of N_2, a 50 mL Schlenk flask with a stirbar was charged with **1** (0.088 g, 0.093 mmol) and 20 mL of CH_2Cl_2. Under an outward flow of N_2, solid [(mnt)$SnMe_2$] (0.029 g, 0.10 mmol) was added to the flask, and the resulting mixture was stirred at ambient temperature for 12 h, during which time a reddish-brown color developed. The solvent was removed under reduced pressure, and the reddish crude solid was then triturated with MeOH (2 × 5 mL), followed by Et_2O (2 × 5 mL), and dried under vacuum. This crude material was further purified on a silica column eluted with CH_2Cl_2 and collected as a red-brown band. Recrystallization was accomplished by the diffusion of MeOH into a filtered $CHCl_3$ solution. Yield: 0.070 g, 74%. R_f = 0.17 (9:1 CH_2Cl_2/hexanes). ^1H NMR ($CDCl_3$): δ 7.37−7.32 (m, 4H, aromatic C−*H*), 7.22−7.12 (m, 21H, aromatic C−*H*), 7.06−6.97 (m, 9H, aromatic C−*H*), 6.90−6.85 (m, 8H, aromatic C−*H*). $^{31}P\{^1H\}$ NMR ($CDCl_3$): δ 57.2 (s), −14.5 (s). UV−vis [CH_2Cl_2; λ_{max}, nm (ε, M^{-1} cm^{-1})]: 366 (4960). IR (KBr, cm^{-1}): 2217 ($\nu_{C\equiv N}$, symm), 2204 ($\nu_{C\equiv N}$, asymm). MS (ESI^+). Calcd for monoisotopic $[C_{58}H_{42}N_2NiP_4S_2]^+$: m/z 1012.1093. Obsd: m/z 1012.1041. Error (δ): 5.2 ppm.

[($Me_2C_2S_2$)Ni(tpbz)] (5). A 50 mL Schlenk flask with a stirbar was charged with **1** (0.088 g, 0.093 mmol) and 20 mL of CH_2Cl_2. Under an outward flow of N_2, solid [($Me_2C_2S_2$)Sn(^{n}Bu)$_2$] (0.0351 g, 0.10 mmol) was added to the flask, which immediately induced a dark-green-brown color. The resulting mixture was stirred at ambient temperature for 12 h. The solvent was removed under reduced pressure, and the solid residual was triturated with MeOH (2 × 5 mL), followed by Et_2O (2 × 5 mL), and then dried under vacuum. This material was purified on a silica chromatography column eluted with CH_2Cl_2/hexanes (9:1) and collected as a green band. Recrystallization was accomplished by the diffusion of *n*-pentane or Et_2O into a filtered CH_2Cl_2 solution. Yield: 0.044 g, 48%. R_f = 0.32 (9:1 CH_2Cl_2/hexanes). ^1H NMR ($CDCl_3$): δ 7.37−7.24 (overlapping m, 12H, aromatic C−*H*), 7.15−7.10 (m, 12H, aromatic C−*H*), 7.03−6.95 (m, 10H, aromatic C−*H*), 6.88−6.84 (m, 8H, aromatic C−*H*), 2.00 (s, 6H, −CH_3). $^{31}P\{^1H\}$ NMR ($CDCl_3$): δ 55.1 (s), −14.9 (s). UV−vis [CH_2Cl_2; λ_{max}, nm (ε, M^{-1} cm^{-1})]: 444 (1440), 638 (160). MS (ESI^+). Calcd for monoisotopic $[C_{58}H_{48}NiP_4S_2]^+$: m/z 990.1501. Obsd: m/z 990.1509. Error (δ): 0.76 ppm.

[($Me_2C_2S_2$)Pd(tpbz)] (6). The same procedure and scale as those described for the synthesis of **4** were implemented but with **2** used in place of the corresponding Ni compound. Purification was accomplished by a chromatography column eluted with CH_2Cl_2/hexanes (3:1), with **5** collected as a yellow band. Yield: 0.032 g, 33%. R_f = 0.20 (9:1 CH_2Cl_2/hexanes). ^1H NMR ($CDCl_3$): δ 7.35−7.25 (m, 12H, aromatic C−*H*), 7.18−7.12 (m, 14H, aromatic C−*H*), 7.06−7.01 (m, 8H, aromatic C−*H*), 6.89−6.84 (m, 8H, aromatic C−H), 2.01 (s, 6H, −CH_3). $^{31}P\{^1H\}$ NMR ($CDCl_3$): δ 49.3 (s), −14.7 (s). UV−vis [CH_2Cl_2; λ_{max}, nm (ε, M^{-1} cm^{-1})]: 427 (1450), 588 (360). MS (ESI^+). Calcd for monoisotopic $[C_{58}H_{48}P_4PdS_2]^+$: m/z 1038.1201. Obsd: m/z 1038.1159. Error (δ): 4.11 ppm.

[($Me_2C_2S_2$)Pt(tpbz)] (7). The same procedure and scale as those described for the synthesis of **4** were implemented but with **3** used in place of the corresponding Ni compound. Purification was accomplished using a silica column chromatography eluted with CH_2Cl_2/hexanes (2:1); **6** was collected as a yellow band. Yield: 0.041 g, 39%. R_f = 0.35 (9:1 CH_2Cl_2/hexanes). ^1H NMR ($CDCl_3$): δ 7.39−7.33 (m, 8H, aromatic C−*H*), 7.29−7.24 (m, 4H, aromatic C−*H*), 7.19−7.13 (m, 14H, aromatic C−*H*), 7.06−7.01 (m, 8H, aromatic C−*H*), 6.90−6.85 (m, 8H, aromatic C−*H*), 2.07 (s, 6H, −CH_3). $^{31}P\{^1H\}$ NMR ($CDCl_3$): δ 44.2 (s, J_{Pt-P}= 2754 Hz), −14.8 (s). UV−vis [CH_2Cl_2; λ_{max}, nm (ε, M^{-1} cm^{-1})]: 418 (3910). MS (ESI^+). Calcd for monoisotopic $[C_{58}H_{48}P_4PtS_2]^+$: m/z 1128.1811. Obsd: m/z 1128.1731. Error (δ): 7.11 ppm.

[($Ph_2C_2S_2$)Ni(tpbz)] (8). A 50 mL Schlenk flask with a stirbar was charged with tpbz (0.081 g, 0.099 mmol) and 20 mL of CH_2Cl_2. Under an outward flow of N_2, [$Ni(S_2C_2Ph_2)_2$] (0.059 g, 0.11 mmol) was added, which quickly induced the formation of a dark-green color. The resulting mixture was stirred for 4 h, after which time the solvent was removed under reduced pressure. The solid residual was purified on a silica column eluted with 2:1 CH_2Cl_2/hexanes, and **8** was isolated as a green band. Following removal of the solvent under reduced pressure, recrystallization of **8** was accomplished by the diffusion of Et_2O vapor into a filtered CH_2Cl_2 or $ClCH_2CH_2Cl$ solution. Continued elution of the column with 10:1 CH_2Cl_2/THF led to a brown band of [(pdt)Ni(tpbz)Ni(pdt)], the properties of which were reported earlier.[2] Yield: 0.059 g, 0.053 mmol, 53%. R_f = 0.82 (9:1 CH_2Cl_2/hexanes). ^1H NMR ($CDCl_3$): δ 7.48−7.42 (m, 8H, aromatic C−*H*), 7.38−7.33 (m, 4H, aromatic C−*H*), 7.24−7.20 (m, 16H, aromatic C−*H*), 7.13−7.08 (m, 10H, aromatic C−*H*), 7.04−7.00 (m, 5H, aromatic C−*H*), 6.97−6.92 (m, 9H, aromatic C−*H*). $^{31}P\{^1H\}$ NMR ($CDCl_3$): δ 55.0 (s), −14.8 (s). UV−vis [CH_2Cl_2; λ_{max}, nm (ε, M^{-1} cm^{-1})]: 416 (3680), 616 (560). MS (ESI^+). Calcd for monoisotopic $[C_{68}H_{52}NiP_4S_2]^+$: m/z 1114.1814. Obsd: m/z 1114.178. Error (δ): 3.08 ppm. Anal. Calcd for **8** ($C_{68}H_{52}NiP_4S_2$): C, 73.19; H, 4.70; P, 11.10. Found: C, 72.99; H, 4.78; P, 11.24.

[($Ph_2C_2S_2$)Pd(tpbz)] (9). The same procedure and scale as those described for **8** were implemented, with the only differences being the onset of a reddish-brown color during the reaction and elution (with 2:1 CH_2Cl_2/hexanes) of the product as a dark-red-purple band from the silica column. Recrystallization was accomplished by the diffusion of Et_2O into a filtered CH_2Cl_2 solution. Continued elution of the column with 10:1 CH_2Cl_2.THF rapidly led to a dark-reddish-orange band of [(pdt)Pd(tpbz)Pd(pdt)], which has been previously described.[2] Yield: 0.060 g, 0.052 mmol, 52%. R_f = 0.73 (9:1 CH_2Cl_2/hexanes). ^1H NMR ($CDCl_3$): δ 7.45−7.34 (m, 11H, aromatic C−*H*), 7.26−7.22 (m, 20H, aromatic C−*H*), 7.13−7.08 (m, 8H, aromatic C−*H*), 7.04−6.92 (m, 13H, aromatic C−*H*). $^{31}P\{^1H\}$ NMR ($CDCl_3$): δ 49.4 (s), −14.7 (s). UV−vis [CH_2Cl_2; λ_{max}, nm (ε, M^{-1} cm^{-1})]: 420 (2670), 544 (860). MS (ESI^+). Calcd for monoisotopic $[C_{68}H_{52}P_4PdS_2]^+$: m/z 1162.1517. Obsd: m/z 1162.1485. Error (δ): 2.77 ppm. Anal. Calcd for **9** ($C_{68}H_{52}PdP_4S_2$): C, 70.19; H, 4.50; P, 10.65. Found: C, 69.57; H, 4.17; P, 9.83.

[($Ph_2C_2S_2$)Pt(tpbz)] (11). Under an atmosphere of N_2, a 50 mL Schlenk flask with a stirbar was charged with tpbz (0.100 g, 0.123 mmol) and CH_2Cl_2 (20 mL). Under an outward flow of N_2, [$Pt(S_2C_2Ph_2)_2$] (0.0834 g, 0.123 mmol) was added, which immediately induced the formation of a blue color. Stirring was continued for 2 h, and the reaction mixture was then kept for 3 days without stirring. The solvent was removed under reduced pressure, and the crude solid residue was purified on a silica column that was flash-eluted with 1:1 CH_2Cl_2/hexanes. The title compound was collected as the leading yellow band. Crystallization of **11** as yellow columns was accomplished by the diffusion of Et_2O vapor into a filtered CH_2Cl_2 solution. Yield: 0.057 g, 37%. R_f = 0.77 (9:1 CH_2Cl_2/hexanes). ^1H NMR ($CDCl_3$): δ 7.60−7.51 (m, 4H, aromatic C−*H*), 7.39−7.36 (m, 10H, aromatic C−*H*), 7.28−7.26 (m, 8H, aromatic C−*H*), 7.06−7.01 (m, 14H, aromatic C−*H*), 6.96−6.89 (m, 16H, aromatic C−*H*). $^{31}P\{^1H\}$ NMR ($CDCl_3$): δ 42.7 (s, J_{Pt-P} = 2742 Hz), −14.9 (s). UV−vis [CH_2Cl_2; λ_{max}, nm (ε, M^{-1} cm^{-1})]: 332 (8750), 399 (2750). MS (ESI^+). Calcd for monoisotopic $[C_{68}H_{52}P_4PtS_2]^+$: m/z 1252.2126. Obsd: m/z 1252.2067. Error (δ): 4.72 ppm. Anal. Calcd for **11** ($C_{68}H_{52}PtP_4S_2$): C, 65.22; H, 4.19. Found: C, 65.22; H, 4.13.

[($Ph_2C_2S_2$)$_2$Pt(tpbz)] (10). Continued elution of the column used for the isolation of compound **11** with 2:1 CH_2Cl_2/hexanes moved **10** as a blue band, which was collected and reduced to dryness. Crystallization of **10** as blue blocks was achieved by the diffusion of Et_2O vapor into a filtered CH_2Cl_2 solution. Yield: 0.017 g, 9%. R_f = 0.23 (9:1 CH_2Cl_2/hexanes), ^1H NMR (CD_2Cl_2): δ 7.64−7.48 (m, 8H, aromatic C−*H*), 7.40−7.19 (m, 16H, aromatic C−*H*), 7.11−7.03 (m, 12H, aromatic C−*H*), 6.96−6.93 (m, 11H, aromatic C−*H*), 6.92−6.84 (m, 9H, aromatic C−*H*), 6.49−6.45 (m, 16H, aromatic

https://doi.org/10.1021/acs.inorgchem.1c01573
Inorg. Chem. 2021, 60, 13177−13192

C−H). $^{31}P\{^1H\}$ NMR (CD_2Cl_2): δ 19.0 (s, J_{Pt-P}= 1787 Hz), −13.3 (s). UV−vis [CH_2Cl_2; λ_{max}, nm (ε, M^{-1} cm^{-1})]: 583 (2140), 355 (11500). MS (ESI^+). Calcd for monoisotopic $[C_{82}H_{62}P_4PtS_4]^+$: *m*/*z* 1494.2349. Obsd: *m*/*z* 1494.229. Error (δ): 3.95 ppm.

[((MeO-*p*-C_6H_4)$_2C_2S_2$)Ni(tpbz)] (12). The same procedure and scale as those described for the synthesis of **8** were implemented but with [((MeO-*p*-C_6H_4)$_2C_2S_2$)$_2$Ni] used in place of [($Ph_2C_2S_2$)$_2$Ni]. Crystals were grown by the diffusion of hexanes vapor into a filtered chlorobenzene solution. Continued elution of the silica column used to purify **12** using 10:1 CH_2Cl_2/THF rapidly moved a brown band of [((MeO-*p*-C_6H_4)$_2C_2S_2$)Ni(tpbz)Ni(S_2C_2(C_6H_4-*p*-OMe)$_2$)], which has been previously described.[2] Yield: 0.057 g of a dark-green solid, 49%. R_f = 0.42 (9:1 CH_2Cl_2/hexanes). ^1H NMR ($CDCl_3$): δ 7.50−7.35 (m, 14H, aromatic C−*H*), 7.26−7.19 (m, 14H, aromatic C−*H*), 7.16−7.10 (m, 11H, aromatic C−*H*), 6.99−6.94 (m, 7H, aromatic C−*H*), 6.63−6.60 (m, 4H, aromatic C−*H*), 3.71 (s, 6H, −O*Me*). $^{31}P\{^1H\}$ NMR ($CDCl_3$): δ 55.2 (s), −14.2 (s). UV−vis [CH_2Cl_2; λ_{max}, nm (ε, M^{-1} cm^{-1})]: 432 (2860), 620 (610). MS (ESI^+). Calcd for monoisotopic $[C_{70}H_{56}NiO_2P_4S_2]^+$: *m*/*z* 1174.2026. Obsd: *m*/*z* 1174.1936. Error (δ): 7.67 ppm. Anal. Calcd for **12** ($[C_{70}H_{56}NiO_2P_4S_2]$): C, 71.50; H, 4.80; P, 10.54; S, 5.45. Found: C, 71.29; H, 4.86; P, 10.41; S, 5.51.

[((MeO-*p*-C_6H_4)$_2C_2S_2$)Pd(tpbz)] (13). The same procedure and scale as those described for the synthesis of **8** were implemented but with [((MeO-*p*-C_6H_4)$_2C_2S_2$)$_2$Pd] used in place of [($Ph_2C_2S_2$)$_2$Ni]. The crude solid residue was purified on a silica column that was flash-eluted with 2:1 CH_2Cl_2/hexanes; **13** was collected as the leading red-purple band. Continued elution with 10:1 CH_2Cl_2/THF rapidly led to a brown-purple band of [((MeO-*p*-C_6H_4)$_2C_2S_2$)Pd(tpbz)Pd-(S_2C_2(C_6H_4-*p*-OMe)$_2$)], which has been previously described.[2] Yield: 0.063 g of a brown-red solid, 52%. R_f = 0.23 (9:1 CH_2Cl_2/hexanes). ^1H NMR ($CDCl_3$): δ 7.47−7.35 (m, 13H, aromatic C−*H*), 7.28−7.21 (m, 16H, aromatic C−*H*), 7.17−7.10 (m, 10H, aromatic C−*H*), 6.99−6.94 (m, 7H, aromatic C−*H*), 6.60−6.30 (m, 4H, aromatic C−*H*), 3.70 (s, 6H, −O*Me*). $^{31}P\{^1H\}$ NMR ($CDCl_3$): δ 49.3 (s), −14.7 (s). UV−vis [CH_2Cl_2; λ_{max}, nm (ε, M^{-1} cm^{-1})]: 432 (2180), 551 (930). MS (ESI^+). Calcd for monoisotopic $[C_{70}H_{56}O_2P_4PdS_2]^+$: *m*/*z* 1221.1729. Obsd: *m*/*z* 1221.1652. Error (δ): 6.23 ppm.

[((MeO-*p*-C_6H_4)$_2C_2S_2$)Pt(tpbz)] (14). The same procedure and scale as those described for the synthesis of **8** were implemented but with [((MeO-*p*-C_6H_4)$_2C_2S_2$)$_2$Pd] used in place of [($Ph_2C_2S_2$)$_2$Ni]. The crude solid residue was purified on a silica column eluted with 2:1 CH_2Cl_2/hexanes, which led to the title compound as the leading yellow band. Continued elution with 10:1 CH_2Cl_2/THF rapidly led to a red band of [((MeO-*p*-C_6H_4)$_2C_2S_2$)Pt(tpbz)Pt(S_2C_2(C_6H_4-*p*-OMe)$_2$)]. Yield: 0.046 g of a bright-yellow solid, 35%. R_f = 0.34 (9:1 CH_2Cl_2/hexanes). ^1H NMR ($CDCl_3$): δ 7.41−7.35 (m, 8H, aromatic C−*H*), 7.29−7.25 (m, 6H, aromatic C−*H*), 7.19−7.10 (m, 16H, aromatic C−*H*), 7.09−7.01 (m, 10H, aromatic C−*H*), 6.90−6.85 (m, 8H, aromatic C−*H*), 3.61 (s, 6H, − O*Me*). $^{31}P\{^1H\}$ NMR ($CDCl_3$): δ 43.8 (s, J_{Pt-P} = 2742 Hz), −14.8 (s). UV−vis [CH_2Cl_2; λ_{max}, nm (ε, M^{-1} cm^{-1})]: 414 (4140). MS (ESI^+). Calcd for monoisotopic $[C_{70}H_{56}O_2P_4PtS_2]^+$: *m*/*z* 1312.2338. Obsd: *m*/*z* 1312.2294. Error (δ): 3.33 ppm.

[($Ph_2C_2S_2$)Pt(tpbz)Ni($S_2C_2Me_2$)] (15). A 50 mL Schlenk flask was charged with [Cl_2Ni(dme)] (0.022 g, 0.1 mmol) and **11** (0.125 g, 0.1 mmol) under a N_2 atmosphere. To this mixture of solids was added CH_2Cl_2 (20 mL) via a syringe, and the resulting solution was stirred at room temperature for 1 h. During this time, a red color appeared. To the same reaction mixture was added [($Me_2C_2S_2$)Sn^nBu_2] (0.035 g, 0.1 mmol), and a deep-red color was generated. The reaction mixture was stirred at ambient temperature overnight (12 h), after which time the solvent was removed under reduced pressure. The resulting dark-red solid residue was triturated with stirring under MeOH (8 mL). This MeOH washing was removed by filter cannulation, and the residue was washed again with MeOH (5 mL), followed by Et_2O (2 × 5 mL). Crude **15** was purified on a silica column eluted with CH_2Cl_2. The red band of **15**, following reduction to dryness, was crystallized from $ClCH_2CH_2Cl$/^{t}BuOMe. Yield: 0.051 g of a red solid, 36%. R_f = 0.18 (CH_2Cl_2). ^1H NMR ($CDCl_3$): δ 7.47−7.41 (m, 18H, aromatic C−*H*), 7.37−7.30 (m, 9H, aromatic C−*H*), 7.24−7.21 (m, 9H, aromatic C−*H*), 7.17−7.13 (m, 11H, aromatic C−*H*), 6.99−6.96 (m, 5H, 2H, aromatic C−*H*), 2.01 (s, 6H, −CH_3). $^{31}P\{^1H\}$ NMR ($CDCl_3$): δ 53.1 (s), 42.3 (s, J_{Pt-P} = 2734 Hz). UV−vis [CH_2Cl_2; λ_{max}, nm (ε, M^{-1} cm^{-1})]: 466 (3940), 733 (1030). MS (ESI^+). Calcd for monoisotopic $[C_{72}H_{58}NiP_4PtS_4]^+$: *m*/*z* 1428.1375. Obsd: *m*/*z* 1428.1367. Error (δ): 0.56 ppm.

[($Ph_2C_2S_2$)Ni(tpbzO$_2$)] (16). In the open air, a solution of **8** (0.111 g, 0.1 mmol) in 15 mL of $CHCl_3$ was treated with a solution of I_2 (0.051 g, 0.2 mmol) in $CHCl_3$ (5 mL). The reaction mixture was stirred overnight (14 h) at ambient temperature. The brownish solution was transferred to a separatory funnel and washed one time with aqueous 1 M NaOH (20 mL). The organic phase was separated as a green solution from the aqueous phase and taken to dryness under reduced pressure to afford crude **16** as a dark-green solid. Further purification was performed by eluting a slurry of the crude mixture with 20:80 THF/$CHCl_3$ from a silica column; **16** led to a green band and was collected and recrystallized from CH_2Cl_2/Et_2O. Yield: 0.044 g of a green solid, 39%. R_f = 0.18 (8:2 CH_2Cl_2/THF). ^1H NMR ($CDCl_3$): δ 7.42−7.36 (m, 10H, aromatic C−*H*), 7.33−7.28 (m, 10H, aromatic C−*H*), 7.26−7.21 (m, 14H, aromatic C−*H*), 7.16−7.12 (m, 13H, aromatic C−*H*), 6.98−6.94 (m, 5H, aromatic C−*H*). $^{31}P\{^1H\}$ NMR ($CDCl_3$): δ 55.8 (s), 29.1 (s). UV−vis [CH_2Cl_2; λ_{max}, nm (ε, M^{-1} cm^{-1})]: 432 (2340), 630 (660). IR (CH_2Cl_2, cm^{-1}): 1245 (vs, $\nu_{P=O}$). MS (ESI^+). Calcd for monoisotopic $[C_{68}H_{52}NiO_2P_4S_2]^+$: *m*/*z* 1146.1713. Obsd: *m*/*z* 1146.1743. Error (δ): 2.62 ppm.

[($Me_2C_2S_2$)Pt(tpbzO$_2$)] (17). In a 25 mL Schlenk tube, [((CH_3)$_2C_2S_2$)Pt(tpbz)] (0.0601 g, 0.0533 mmol) was dissolved in CH_2Cl_2 (3 mL) under N_2. To this solution was added H_2O_2 (0.02 mL, 30% in H_2O, 0.2 mmol), and the mixture was stirred at room temperature overnight. The solvent and all volatiles were removed under reduced pressure, and the solid residual was redissolved in a minimal volume of CH_2Cl_2. To this CH_2Cl_2 solution were added hexanes (15 mL) to induce precipitation of an orange solid, which was then isolated by filtration and washed with hexanes (3 × 5 mL). Recrystallization of **17** as orange needles was accomplished by the diffusion of Et_2O vapor into a CH_2Cl_2 solution. Yield: 0.0245 g, 40%. ^1H NMR ($CDCl_3$): δ 7.47−7.21 (m, 42H, aromatic C−*H*), 2.15 (s, 6H, CH_3). $^{31}P\{^1H\}$ NMR ($CDCl_3$): δ 45.1 (s, *P*Ph_2Pt, J_{P-Pt} = 2755 Hz), 29.0 (s, *P*Ph_2O). MS (ESI^+). Calcd for monoisotopic $[C_{58}H_{48}O_2P_4PtS_2]^{1+}$: *m*/*z* 1160.1604. Obsd: *m*/*z* 1160.1709. Error (δ): 9.05 ppm.

[($Me_2C_2S_2$)Ni(tpbzS$_2$)] (18). A solution of [((CH_3)$_2C_2S_2$)Ni-(tpbz)] (0.0477 g, 0.048 mmol) in THF (3.6 mL) was treated with $[NH_4]_2S$ (0.60 mL, 20% in H_2O) and then allowed to stir at ∼50 °C for 3 days. The mixture was reduced to dryness under reduced pressure, redissolved in a minimal volume of $CHCl_3$, and eluted from a silica column packed as a slurry in $CHCl_3$. The leading green-brown band was collected and reduced to dryness, yielding **18** as a brown solid. Yield: 0.0223 g, 38%. ^1H NMR ($CDCl_3$): δ 7.51−7.30 (m, 26H, aromatic C−*H*), 7.30−7.16 (m, 16H, aromatic C−*H*), 2.06 (s, 6H, −CH_3). ^{31}P NMR ($CDCl_3$): δ 55.9 (s, −Ph_2*P*Ni), 46.9 (s, −Ph_2*P*S). UV−vis [CH_2Cl_2; λ_{max}, nm (ε, M^{-1} cm^{-1})]: 448 (2270). MS (ESI^+). Calcd for monoisotopic $[C_{58}H_{48}NiP_4S_4]^+$: *m*/*z* 1054.0943. Obsd: *m*/*z* 1054.0951. Error (δ): 0.82 ppm. Anal. Calcd for **18** ($[C_{58}H_{48}NiP_4S_4]$): C, 65.98; H, 4.58; P, 11.73. Found: C, 65.46; H, 4.44; P, 10.7.

[Ni(dppbO$_2$)$_3$][I_3]$_2$ ([19][I_3]$_2$). Under an atmosphere of N_2, a 50 mL Schlenk flask with a stirbar was charged with Ni(NO_3)$_2$ (0.013 g, 0.039 mmol) and THF (20 mL). Under an outward flow of N_2, solid dppbO_2 (0.056 mg, 0.117 mmol) was added in a single portion, which induced the development of a very light-green solution. The reaction mixture was stirred overnight (14 h) at ambient temperature. Cesium triiodide (0.040 g, 0.078 mmol) was added under an outward flow of N_2, followed by the addition of MeOH (2 mL). The resulting red-brown solution was stirred for 5 h at ambient temperature. Under reduced pressure, the solution was concentrated to a volume of ∼3 mL, whereupon Et_2O (10 mL) was added to precipitate the crude

https://doi.org/10.1021/acs.inorgchem.1c01573
Inorg. Chem. 2021, 60, 13177−13192

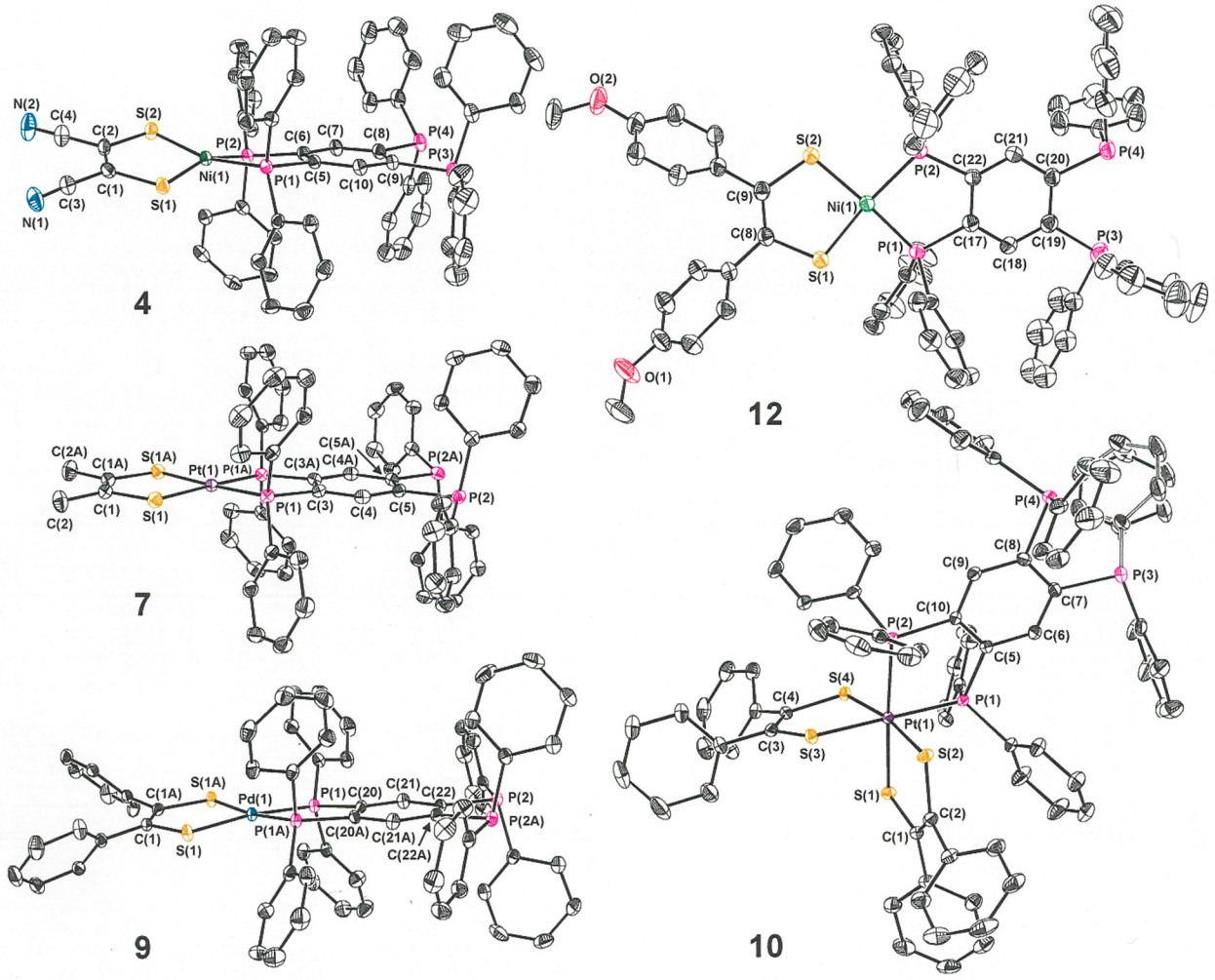

Figure 2. Thermal ellipsoid plots (50% probability level) of selected open-ended tpbz compounds that have been characterized by X-ray crystallography. All H atoms have been omitted for clarity.

product as a red-brown powder. The solvent was removed by cannula filtration, and the dark red-brown solid residue was washed with Et_2O (3 × 5 mL) and dried under vacuum. Diffraction-quality red-orange plate crystals were grown by diffusion of Et_2O into a filtered concentrate of the complex in CH_2Cl_2. Yield: 0.076 g, 87%. UV−vis [CH_2Cl_2; λ_{max}, nm (ε, M^{-1} cm^{-1})]: 426 (8920). Solution IR (CH_2Cl_2, cm^{-1}): 1264 (vs, $\nu_{P=O}$). MS (ESI^+). Calcd for monoisotopic $[C_{90}H_{72}NiP_6S_6]^+$: m/z 1492.3108. Calcd for $[C_{90}H_{72}NiP_6S_6]^{2+}$: m/z 746.1554. Obsd: m/z 746.1566. Error (δ): 1.65 ppm.

DISCUSSION

Syntheses and Structures. Charge-neutral homoleptic bis(dithiolene) complexes of the Group 10 metals $[M(S_2C_2R_2)_2]$ (M = Ni^{2+}, Pd^{2+}, Pt^{2+}) are subject to direct displacement of one ligand by soft σ donors such as phosphines or isocyanides. When the tpbz ligand is introduced to $[M(S_2C_2R_2)_2]$ in a 1:1 ratio, the open-ended $[[(R_2C_2S_2)M(tpbz)]$ compounds are efficiently generated in yields ranging from ∼30 to 50% (Scheme 2, Method 2). Purification by column chromatography and crystallization from dry solvents by vapor diffusion methods are straightforward. The Pt complexes proceed through an octahedral bis(dithiolene)-diphosphine intermediate that is isolable in minor amounts (cf. **10**, Scheme 2). Because the cyano-substituted dithiolene ligand does not support stable $[M(S_2C_2(CN)_2)_2]^0$ complexes that can extrude a dithiolene ligand, the $[((NC)_2C_2S_2)M(tpbz)]$ complexes must be prepared by the alternate route of transmetalation using a dialkyltin dithiolene complex (Scheme 2, Method 1). Method 1 has demonstrated usefulness in chloride-for-dithiolene ligand exchange for a broad variety of dithiolene ligand types.[2,12−18] The open-ended $[Cl_2M(tpbz)]$ compounds (**1**−**3**) with which these transmetalation reactions occur are themselves new compounds and are readily obtained in ∼80−90% yields by the introduction of tpbz to $[Cl_2Ni(dme)]$ or $[Cl_2M(N{\equiv}CCH_3)_2]$ (M = Pd, Pt). All open-ended tpbz compounds are spectroscopically distinct by ^{31}P NMR from the symmetric, dimetallic compounds because they display a signal upfield of the H_3PO_4 reference, which is ascribed to the open end, and a signal ∼50 ppm downfield of the reference, which arises from the P atoms chelated to M^{2+}.

Representative members of the set of new compounds summarized in Scheme 2 have been characterized by X-ray crystallography (Figure 2 and Tables 1 and 2). In contrast to the dimetallic compounds $[(R_2C_2S_2)M(tpbz)M(S_2C_2R_2)]$, which show a proclivity to crystallize upon an inversion center in monoclinic $P2_1/c$ (No. 14), the structures of the compounds in Scheme 2 reveal a tendency to coincide with C_2 axes in monoclinic $C2/c$ (No. 15). As is typical for the d^8 configuration, compounds **1**−**5**, **7**−**10**, and **11** display structures that are best described as square-planar, albeit

https://doi.org/10.1021/acs.inorgchem.1c01573
Inorg. Chem. 2021, 60, 13177−13192

Table 2. Unit Cell and Refinement Data for Compounds Characterized by X-ray Diffraction

compound	[(adt)Ni(tpbz)]	[(pdt)Pt(tpbz)Ni(mdt)]	[(pdt)Ni(tpbzO$_2$)]	[(mdt)Pt(tpbzO$_2$)]
compound no.	**12**	**15**	**16**	**17**
cocryst solvent	none	$2^1/_2$(ClCH$_2$CH$_2$Cl)	CH$_2$Cl$_2$	none
formula	$C_{70}H_{56}NiO_2P_4S_2$	$C_{77}H_{68}Cl_5NiP_4PtS_4$	$C_{69}H_{54}Cl_2NiO_2P_4S_2$	$C_{58}H_{48}O_2P_4PtS_2$
fw, g mol^{-1}	1175.85	1676.48	1232.73	1160.05
temperature, K	150	150	150	150
wavelength, Å	1.54178	0.71073	0.71073	0.71073
2θ range, deg	4.59−144.21	3.87−66.84	3.57−61.23	4.18−66.45
cryst syst	monoclinic	triclinic	triclinic	monoclinic
space group	$P2_1/n$	$P\bar{1}$	$P\bar{1}$	$P2_1/c$
a, Å	12.0422(4)	12.5374(6)	13.4505(18)	17.0751(11)
b, Å	38.5014(13)	12.5692(6)	16.597(2)	16.0625(10)
c, Å	14.0003(6)	24.7673(13)	16.653(2)	20.5241(13)
α, deg	90	92.953(2)	64.068(4)	90
β, deg	112.798(2)	91.560(2)	70.817(4)	108.283(2)
γ, deg	90	108.166(2)	72.092(4)	90
volume (Å^3), Z	5984.0(4), 4	3699.6(3), 2	3098.4(7), 2	5345.0(6), 4
density, g cm^{-3}	1.305	1.505	1.321	1.442
μ, mm^{-1}	2.484	2.565	0.615	2.864
color, habit	yellow-green plate	orange plate	orange plate	dark-orange column
limiting indices h	$-14 \le h \le 14$	$-19 < h < 19$	$-19 < h < 19$	$-26 \le h \le 26$
limiting indices k	$-44 \le k \le 46$	$-19 < k < 19$	$-23 < k < 23$	$-24 \le k \le 24$
limiting indices l	$-16 \le l \le 14$	$0 < l < 38$	$-23 < l < 23$	$-31 \le l \le 31$
reflns collected	51648	32993	144627	403235
indep data, param[a]	11399, 703	32993, 856	19027, 728	20472, 606
GOF[b]	1.039	1.277	1.044	1.081
R1,[c,d] wR2[d,e]	0.0479, 0.1008	0.0751, 0.1691	0.0488, 0.1165	0.0239, 0.0594
R1,[c,f] wR2[e,f]	0.0699, 0.1106	0.0827, 0.1717	0.0878, 0.1350	0.0314, 0.0641
compound	[(mdt)Ni(tpbzS$_2$)]	[(dppbO$_2$)$_3$Ni][I$_3$]$_2$	[(dppbO$_2$)$_3$Ni][I$_3$]$_2$	
compound no.	**18**	[**19**][I$_3$]$_2$	[**19**][I$_3$]$_2$	
cocryst solvent	none	none	none	
formula	$C_{58}H_{48}NiP_4S_4$	$C_{90}H_{72}I_6NiO_6P_6$	$C_{90}H_{72}I_6NiO_6P_6$	
fw, g mol^{-1}	1055.79	2255.41	2255.40	
temperature, K	100	100	150	
wavelength, Å	0.71073	0.71073	0.71073	
2θ range, deg	2.46−49.52	3.12−54.00	3.628−46.660	
cryst syst	monoclinic	triclinic	monoclinic	
space group	$P2_1/c$	$P\bar{1}$	$P2_1/c$	
a, Å	9.3284(12)	13.0484(12)	15.0552(10)	
b, Å	30.386(4)	13.3478(12)	26.0258(18)	
c, Å	19.858(3)	26.880(3)	22.6547(15)	
α, deg	90	102.137(1)	90	
β, deg	98.487(2)	92.504(1)	101.217(2)	
γ, deg	90	106.961(1)	90	
volume (Å^3), Z	5567.1(13), 4	4350.1(7), 2	8707.1(10), 4	
density, g cm^{-3}	1.260	1.722	1.721	
μ, mm^{-1}	0.649	2.514	2.512	
color, habit	yellow needle	orange plate	orange-red plate	
limiting indices h	$-10 \le h \le 10$	$-16 \le h \le 16$	$-15 \le h \le 16$	
limiting indices k	$-35 \le k \le 35$	$-17 \le k \le 17$	$-28 \le k \le 28$	
limiting indices l	$-23 \le l \le 23$	$-34 \le l \le 34$	$-25 \le l \le 25$	
reflns collected	39326	37066	153572	
indep data, param[a]	9510, 610	18761, 985	12505, 989	
GOF[b]	0.964	0.945	1.023	
R1,[c,d] wR2[d,e]	0.0898, 0.1686	0.0427, 0.0931	0.0505, 0.1241	
R1,[c,f] wR2[e,f]	0.1753, 0.2007	0.0707, 0.1017	0.0794, 0.1403	

[a]Independent data collected and parameters refined. [b]GOF = $\{\sum[w(F_o^2 - F_c^2)^2]/(n-p)\}^{1/2}$, where n = number of reflections and p is the total number of parameters refined. [c]R1 = $\sum||F_o| - |F_c||/\sum|F_o|$. [d]$R$ indices for data cut off at $I > 2\sigma(I)$. [e]wR2 = $\{\sum[w(F_o^2 - F_c^2)^2]/\sum[w(F_o^2)^2]\}^{1/2}$; $w = 1/[\sigma^2(F_o^2) + (xP)^2 + yP]$, where $P = [2F_c^2 + \mathrm{Max}(F_o^2,0)]/3$. [f]$R$ indices for all data.

with minor tetrahedral distortions. Quantified by the angle θ between the S−M−S and P−M−P planes, these departures from ideal planarity are more pronounced for the Ni complexes than for the heavier metal complexes (Table 3).

https://doi.org/10.1021/acs.inorgchem.1c01573
Inorg. Chem. 2021, 60, 13177−13192

Table 3. Selected Interatomic Distances, Bond Angles, And Other Structural Parameters for Compounds 1, 4, 5, 7, [(pdt)M(η^2-tpbz)] (M = Ni, 8; Pd, 9; Pt, 11), and 12[a]

	1	4	5	7	8	9	11	12
M−X[b]	2.1814[8]	2.1489[6]	2.1494(6)	2.2933(8)	2.1518(5)	2.2935(6)	2.2993(8)	2.1457[6]
M−P[c]	2.1320[8]	2.1542[6]	2.1620(6)	2.2431(8)	2.1712(8)	2.2713(2)	2.2521(9)	2.1503[6]
Δ,[d] Å		0.0053	0.0126	−0.0502	0.0194	−0.0222	−0.0472	0.0046
S−C		1.738[2]	1.765(2)	1.760(3)	1.7568(16)	1.767(2)	1.767(3)	1.757[2]
$_{S-}C{=}C_{-S}$		1.353(5)	1.333(5)	1.327(6)	1.346(3)	1.340(5)	1.348(7)	1.353(4)
P−C_{bound}[e]	1.814[3]	1.813[2]	1.827(2)	1.822(3)	1.8242(16)	1.825(2)	1.820(3)	1.827[2]
P−C_{open}[f]	1.852[3]	1.848[2]	1.848(2)	1.849(3)	1.8449(16)	1.849(2)	1.840(3)	1.843[2]
md,[g] Å	0.144	0.267	0.070	0.035	0.125	0.112	0.112	0.243
δ,[h] Å	0.019	0.028	0.000	0.000	0.000	0.000	0.000	0.056
X−M−X[b]	94.73(5)	93.62(3)	90.83(3)	88.16(4)	90.89(2)	88.35(3)	88.04(4)	91.71(3)
P−M−P[c]	88.68(2)	87.65(3)	89.38(3)	87.74(4)	88.64(4)	86.50(3)	86.80(4)	89.57(3)
X−M−P_{cis}[b]	89.04[4]	92.00[2]	90.08(2)	92.09(3)	90.827(14)	93.01(2)	93.01(3)	89.68[2]
X−M−P_{trans}[b]	169.96[4]	162.19[3]	175.30(2)	177.75(3)	171.658(16)	172.88(8)	172.92(3)	163.90[3]
θ,[i] deg	13.1	24.9	6.6	3.2	11.7	10.2	10.2	22.5
φ,[j] deg	3.5	7.2	1.2	1.2	2.6	2.4	2.5	1.9

[a]Averaged values are given where two or more chemically identical interatomic distances or angles are present. Uncertainties are propagated according to Taylor, J. R. *An Introduction to Error Analysis*, 2nd ed.; University Science Books: Sausalito, CA, 1997; pp 73−77; propagated uncertainties are designated with [ ]. [b]M = Ni, X = Cl; M = Ni, Pd, or Pt and X = S. [c]M = Ni, Pd, or Pt. [d]Δ = M−P − M−S bond length difference. [e]C atom of the central arene ring, metalated side. [f]C atom of the central arene ring, open side. [g]md = mean atom deviation from the X_2MP_2 plane. [h]δ = deviation (Å) of M from the X_2MP_2 plane. [i]Angle between the S_2M and P_2M planes. [j]Angle between the MP_2 and $P_2C_6P_2$ mean planes.

Table 4. Selected Bond Lengths (Å) and Angles (deg) for 10[a]

$C{=}C_{dithiolene,chelate}$	1.348[3]
C−S	1.771[2]
Pt−$S_{cis\ to\ P}$	2.3688[5]
Pt−$S_{trans\ to\ P}$	2.3607[5]
Pt−P	2.3373[5]
S(2)−Pt(1)−S(4)	170.34(2)
S−Pt−$S_{intraligand}$	88.63[1]
S(1)−Pt(1)−S(3)	91.23(3)
S−Pt−S[b]	84.63[1]
P−Pt−P	86.09(2)
φ[c]	15.9

[a]Averaged values are given where two or more chemically identical interatomic distances or angles are present. Uncertainties are propagated according to Taylor, J. R. *An Introduction to Error Analysis*, 2nd ed.; University Science Books: Sausalito, CA, 1997; pp 73−77; propagated uncertainties are designated with [ ]. [b]Interligand S−Pt−S, with one S atom in the PtP_2 plane and one orthogonal to it. [c]φ = angle between the PtP_2 plane and $P_2C_6P_2$ mean plane.

A longer M−P then M−S bond length is observed in all Ni compounds, while the inverse is true is for the Pd and Pt complexes. This same pattern is clearly evident in the $[(R_2C_2S_2)M(tpbz)M(S_2C_2R_2)]$ compounds and has been attributed to more effective metal d − sulfur p σ overlap in the HOMO−3 and HOMO−4 for Ni versus Pd and Pt.[2] Undoubtedly, this explanation is equally pertinent to the open-ended compounds. The P−C bond lengths to the central arene ring of the tpbz ligand differ notably between the bound and open ends of the ligand. A consistently longer P−C bond, by ∼0.02 Å, is found at the open end.

Bis(dithiolene)diphosphine compound **10** is an intermediate on the pathway toward **11** and is isolable in varying amounts depending the temperature and length of the reaction time. Compound **10** occurs as a result of an atypical oxidative addition reaction, wherein the two electrons from Pt^{II} in $[(Ph_2C_2S_2)_2Pt]$ are distributed to the dithiolene radical monoanions (**b** → **a**, Scheme 1), thereby reducing them to ene-1,2-dithiolates rather than to the incoming ligand (diphosphine), as is usually the case. The subsequent transformation of **10** to **11** is a reductive elimination that extrudes one dithiolene ligand in a highly reactive fully oxidized form (**c** or possibly **d**, Scheme 1) and restores the Pt^{II} redox state. In related systems, trapped forms of this expelled dithiolene ligand, e.g., as a 1,2,5,6-tetrathiocin[19] or as a 1,3-dithiol-2-alkylimine,[20] affirm this general accounting of the redox transaction. The crystal structure of **10** (Figure 2) establishes the octahedral geometry that is common for Pt^{IV}, with both dithiolene ligands in the fully reduced ene-1,2-dithiolate redox level, as gauged by S−C and $C{-}C_{chelate}$ bond lengths (Table 4). These S−C and $C{-}C_{chelate}$ bond lengths are markedly longer and shorter, respectively, than those in the initial $[(Ph_2C_2S_2)_2Pt]$ complex. Furthermore, UV−vis and X-ray absorption spectroscopic measurements of very similar platinum dithiolenebis(phosphine) complexes[21] are consistent with the foregoing descriptions of the redox changes and molecular electronic structure.

Heterodimetallic compound **15** is readily prepared either by the treatment of **11** with $[(Me_2C_2S_2)_2Ni]$ or by the reaction between **5** and $[(Ph_2C_2S_2)_2Pt]$ (Scheme 3). This flexibility in the approach to the synthesis is enabled by the robust character of the open-ended tpbz compounds and offers a glimmer of future possibilities for "modular" synthesis. The structure of **15** (Figure 3 and Table 5) reveals bond lengths and other parameters that are consistent with independent, noninteracting metal centers. For example, the Δ_M values (the difference between the M−P and M−S average bond lengths) are negative and positive, respectively, for Pt and Ni, as found for the analogous homodimetallic compounds.[2] The Ni center reveals a slight tetrahedralization (φ = 11.4°) compared to the more planar environment around Pt (φ = 3.4°).

As suggested by the synthesis of **15**, the open-ended compounds of Scheme 2 are themselves phosphine ligands that should broadly manifest the reactivity associated with this ligand type. As one example, without detriment to the

https://doi.org/10.1021/acs.inorgchem.1c01573
Inorg. Chem. 2021, 60, 13177−13192

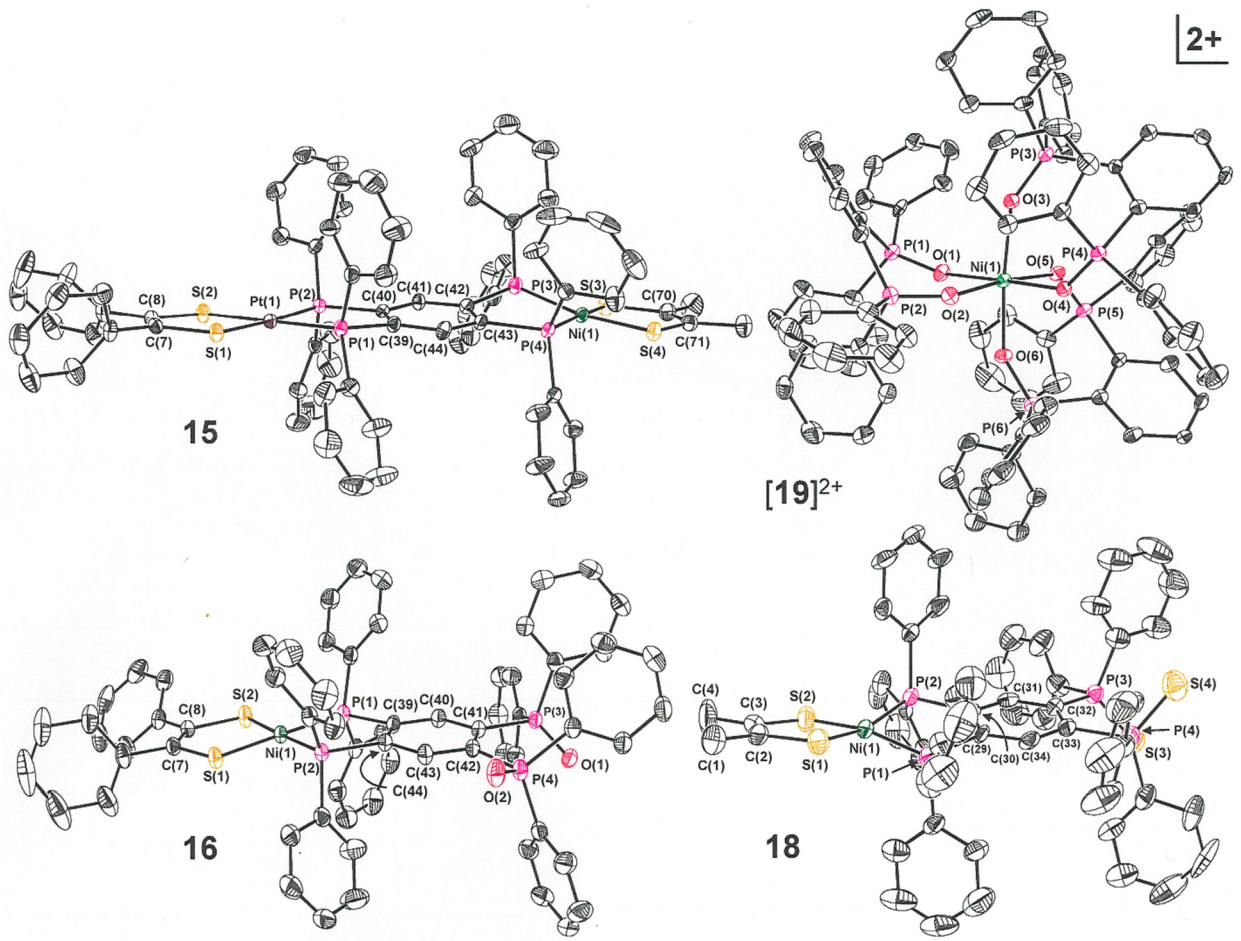

Figure 3. Thermal ellipsoid plots (50% probability level) of dimetallic **15**, open-ended oxidized **16** and **18**, and mononuclear $[\mathbf{19}]^{2+}$ from X-ray crystallographic characterization. All H atoms have been omitted for clarity.

Table 5. Selected Interatomic Distances (Å) and Angles (deg) for 15[a]

Pt−S	2.2921[12]	S−Pt−S	88.81(6)
Pt−P	2.2461[12]	P−Pt−P	87.43(6)
Δ_{Pt}[b]	−0.046	S−Pt−P_{cis}	91.88[4]
Ni−S	2.142[1]	S−Pt−P_{trans}	177.68[5]
Ni−P	2.1535[13]	θ_1,[c] deg	3.4
Δ_{Ni}[b]	+0.012	S−Ni−S	91.21(8)
S−C_{pdt}	1.758[4]	P−Ni−P	88.07(7)
S−C_{mdt}	1.751[5]	S−Ni−P_{cis}	90.82[5]
C═C_{pdt}	1.350(9)	S−Ni−P_{trans}	171.68[6]
C═C_{mdt}	1.352(11)	θ_2,[c] deg	11.4
Pt···Ni, Å	8.811		

[a]Averaged values are given where two or more chemically identical interatomic distances or angles are present. Uncertainties are propagated according to Taylor, J. R. *An Introduction to Error Analysis*, 2nd ed.; University Science Books: Sausalito, CA, 1997; pp 73−77; propagated uncertainties are designated with [ ]. [b]Δ_M = (M−P) − (M−S) bond length difference. [c]θ = angle between the S_2M and P_2M planes.

Table 6. Selected Interatomic Distances (Å), Bond Angles (deg), and Other Structural Parameters for 16−18[a]

	[$(Ph_2C_2S_2)$Ni(tpbzO_2)]	[$(Me_2C_2S_2)$Pt(tpbzO_2)]	[$(Me_2C_2S_2)$Ni(tpbzS_2)]
M−S	2.1477[5]	2.2934[4]	2.137[1]
M−P	2.1656[5]	2.2588[3]	2.141[1]
Δ[b]	+0.0179	−0.0346	+0.004
S−C	1.759[1]	1.759[1]	1.755[6]
P−C^c	1.833[1]	1.8247[12]	1.836[5]
P−C^d	1.840[1]	1.8323[12]	1.848[5]
P═E	1.4931[12]	1.4936[11]	1.929[2]
S−M−S	90.86(2)	88.006(18)	92.13(9)
P−M−P	89.42(2)	86.717(16)	89.95(8)
S−M−P_{cis}	89.83[1]	93.265[12]	91.06[6]
S−M−P_{trans}	177.76[2]	171.307[12]	164.34[6]
θ,[e] deg	2.3	12.3	22.1
φ,[f] deg	5.5	19.1	7.9

[a]Averaged values are given where two or more chemically identical interatomic distances or angles are present. Uncertainties are propagated according to Taylor, J. R. *An Introduction to Error Analysis*, 2nd ed.; University Science Books: Sausalito, CA, 1997; pp 73−77; propagated uncertainties are designated with [ ]. [b]Δ = (M−P) − (M−S) bond length difference. [c]C atom of the central arene ring, metalated side. [d]C atom of the central arene ring, open side. [e]Angle between the S_2M and P_2M planes. [f]Angle between the MP_2 plane and $P_2C_6P_2$ mean plane.

metalated end of tpbz, the open phosphine groups can undergo oxidative addition of the chalcogen atom to form the corresponding phosphine oxides or sulfides. Several representative compounds—[$(Ph_2C_2S_2)$Ni(tpbzO_2)], [$(Me_2C_2S_2)$Pt(tpbzO_2)], and [$(Me_2C_2S_2)$Ni(tpbzS_2)]—have been prepared in a straightforward fashion using I_2/air, H_2O_2, $[NH_4]_2[S]$,

https://doi.org/10.1021/acs.inorgchem.1c01573
Inorg. Chem. 2021, 60, 13177−13192

Scheme 4. Preparation of $[Ni(dppbO_2)_3][I_3]_2$

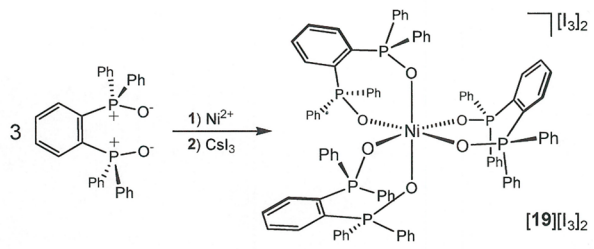

respectively. For reasons not immediately obvious, the known I_2/air protocol[11] that works to produce **16** in modest yield appears to be ineffective in generating the Pt compound **17**. However, the more vigorous H_2O_2 effectively oxidizes **7** to afford **17** in a yield comparable to the production of **16** from **8** by I_2/air. Considering the reported susceptibility of [(bdt)Pt(bipy)] to complete oxidation of the thiolate S atoms to the disulfinate form in the presence of light and O_2,[22] it is somewhat surprising that the often indiscriminate H_2O_2 can produce **17** without significant attending decomposition. These several oxidized compounds are readily distinguished by ^{31}P NMR spectroscopy from the open-ended $[(R_2C_2S_2)M(tpbz)]$ compounds because the signal arising from the trivalent P is moved 40−60 ppm downfield and nearer to the signal arising from the P nuclei bound to M^{2+}. Structurally, **16**−**18** are similar to **5**−**9** and **11** in having closer adherence to planarity for the heavier metal, positive and negative Δ (Table 6) for the Ni and Pt compounds, respectively, and modestly longer $P-C_{central\ arene}$ bond lengths at the open end versus the metalated end. The bond lengths from P to terminal chalogenide are typically at ∼1.49 Å for the oxide[23,24] and ∼1.93 Å for the sulfide.[25,26]

The potential utility of compounds such as **17** and **18** is: (1) Their capacity to select different ions at their open end versus $[(R_2C_2S_2)M(tpbz)]$ by virtue of the ylide character to the phosphine sulfide or oxide; (2) their ability to form homoleptic tris(chelate) complexes because the otherwise prohibitive congestion that would be occasioned by six Ph_2P groups is further removed from the coordination sphere of M^{n+}. Such possibilities are intimated by the finding that a test reaction between the related $dppbO_2$ and Ni^{2+} leads to octahedral $[(dppbO_2)_3Ni]^{2+}$, which has been isolated as its I_3^- salt (Scheme 4 and Figure 3) in both triclinic and monoclinic forms. Selected structural parameters, which are highly similar for both polymorphs, are presented in Table S5. The phosphoryl P−O bond lengths in $[\mathbf{19}]^{2+}$ (1.491[1] Å) are slightly longer than those in the free ligand (1.485[1] Å).[24] Each ligand shows a substantial folding around the intraligand O···O axis such that the NiO_2 plane meets the $P_2C_{2\ chelate}$ mean plane at an angle of ∼57° (average of six values). For both structures of $[\mathbf{19}]^{2+}$, the directionality of this folding is different for one $dppbO_2$ ligand than it is for the other two, thus lowering the symmetry from C_3 to C_1. These structures for $[\mathbf{19}]^{2+}$ appear to be the first for a homoleptic tris(chelate) coordination complex with $dppbO_2$, although a preparation of the $[(dppbO_2)_3M]^{2+}$ (M = Mg^{2+}, Ca^{2+}, Sr^{2+}, Ba^{2+}) series has been reported.[27] A related tris(chelate) of Ni^{2+}, $[(dppeO_2)_3Ni]^{2+}$ ($dppeO_2$ = 1,2-bis(diphenylphosphino)-ethane dioxide), has been structurally authenticated[28] but notably contrasts with $[\mathbf{19}]^{2+}$ in having a much more modest average angle of 9.2° between the NiO_2 and $P_2C_{2\ chelate}$ planes for its ligands.

Electrochemistry. The open-ended compounds $[(R_2C_2S_2)M(tpbz)]$ generally support a reversible $1e^-$ oxidation that is attributed to transformation of the ene-1,2-dithiolate dianion into its radical monoanionic form (Scheme 1, **a** → **b**). The potential at which this oxidation occurs is shifted cathodically by ∼0.050 V compared to the corresponding feature in the symmetric, dimetallic complex. This modest shift appears to be due to an inherent electron-donating character of the tetraphosphino ligand platform, which is tempered somewhat when the ligand's open end chelates a second $M(S_2C_2R_2)$ group. However, the second reversible oxidation that occurs in $[(R_2C_2S_2)M(tpbz)M(S_2C_2R_2)]$ (M = Ni, Pd, Pt; R = Ph, *p*-anisyl) is typically irreversible in their open-ended counterparts (Table 7). In $[(R_2C_2S_2)M(tpbz)M(S_2C_2R_2)]$, this second wave was assigned to radical monoanion to α-dithione oxidation (Scheme 1, **b** → **c**). Assuming a similar description pertains to the open-ended

Table 7. Electrochemical Data (V) for the Open-Ended Compounds 4−6 and 8−15 for Dimetallic tpbz-Bridged 15 and for Open-Ended Oxidized 16 versus Cp_2Fe^+/Cp_2Fe with a 0.10 M $[Bu_4N][PF_6]$ Supporting Electrolyte, a Glassy Carbon or Pt Disk Working Electrode, and CH_2Cl_2 as the Solvent[a]

	E_4(ox)	E_3(ox)	E_2(ox)	E_1(ox)	E_1(red)
[(mnt)Ni(tpbz)][b], **4**				+0.62 (ir, 1e)[d]	−1.53 (r, 1e)[e]
[(mdt)Ni(tpbz)][c], **5**			+0.71 (ir, 1e)[d]	0.00 (r, 1e)[e]	−2.11 (qr, 1e)[f]
[(mdt)Pt(tpbz)][c], **6**		+0.85 (ir)[g]	+0.66 (ir)[g]	−0.01 (r, 1e)[e]	
[(pdt)Ni(tpbz)][c], **8**			+0.71 (ir, 1e)[e]	+0.09 (r, 1e)[e]	−2.10 (r, 1e)[e]
[(pdt)Pd(tpbz)][c], **9**		+0.85 (ir, 1e)[d]	∼+0.66 (ir, 1e)[d]	+0.05 (r, 1e)[e]	
[(pdt)Pt(tpbz)][c], **11**		+0.88 (qr, 1e)[e]	+0.54 (ir, 1e)[d]	+0.13 (r, 1e)[e]	−1.97 (qr, 1e)[f]
[$(pdt)_2$Pt(tpbz)][b], **10**	+0.66 (ir)[g]	+0.48 (r, 1e)[e]	+0.16 (qr, 1e)[f]	−0.02 (r, 1e)[e]	−1.22 (ir)[g]
[(adt)Ni(tpbz)][c], **12**			+0.59 (qr, 1e)[f]	+0.02 (r, 1e)[e]	−2.11 (qr, 1e)[f]
[(adt)Pd(tpbz)][c], **13**			+0.67 (ir, 1e)[d]	+0.09 (r, 1e)[e]	
[(adt)Pt(tpbz)][c], **14**			+0.60 (qr, 1e)[f]	+0.01 (r, 1e)[e]	
[(pdt)Pt(tpbz)Ni(mdt)][c], **15**	+0.92 (r, 1e)[e]	+0.70 (r, 1e)[e]	+0.19 (r, 1e)[e]	+0.06 (r, 1e)[e]	−1.97 (r, 1e)[e]
[(pdt)Ni(tpbzO_2)][c], **16**			+0.75 (qr, 1e)[f]	0.12 (r, 1e)[e]	−1.98 (r, 1e)[e]

[a]Ligand abbreviations: mnt = $[(NC)_2C_2S_2]^{2-}$, mdt = $[Me_2C_2S_2]^{2-}$, pdt = $[Ph_2C_2S_2]^{2-}$, and adt = $[(MeO\text{-}p\text{-}C_6H_4)_2C_2S_2]^{2-}$. [b]A Pt disk working electrode was used. [c]A glassy carbon working electrode was used. [d]ir = irreversible; value obtained by differential pulse voltammetry. [e]r = reversible; value obtained by cyclic voltammetry. [f]qr = quasireversible; value obtained by cyclic voltammetry. [g]ir = irreversible; value estimated from the anodic maximum, E_a, in the cyclic voltammogram.

https://doi.org/10.1021/acs.inorgchem.1c01573
Inorg. Chem. 2021, 60, 13177−13192

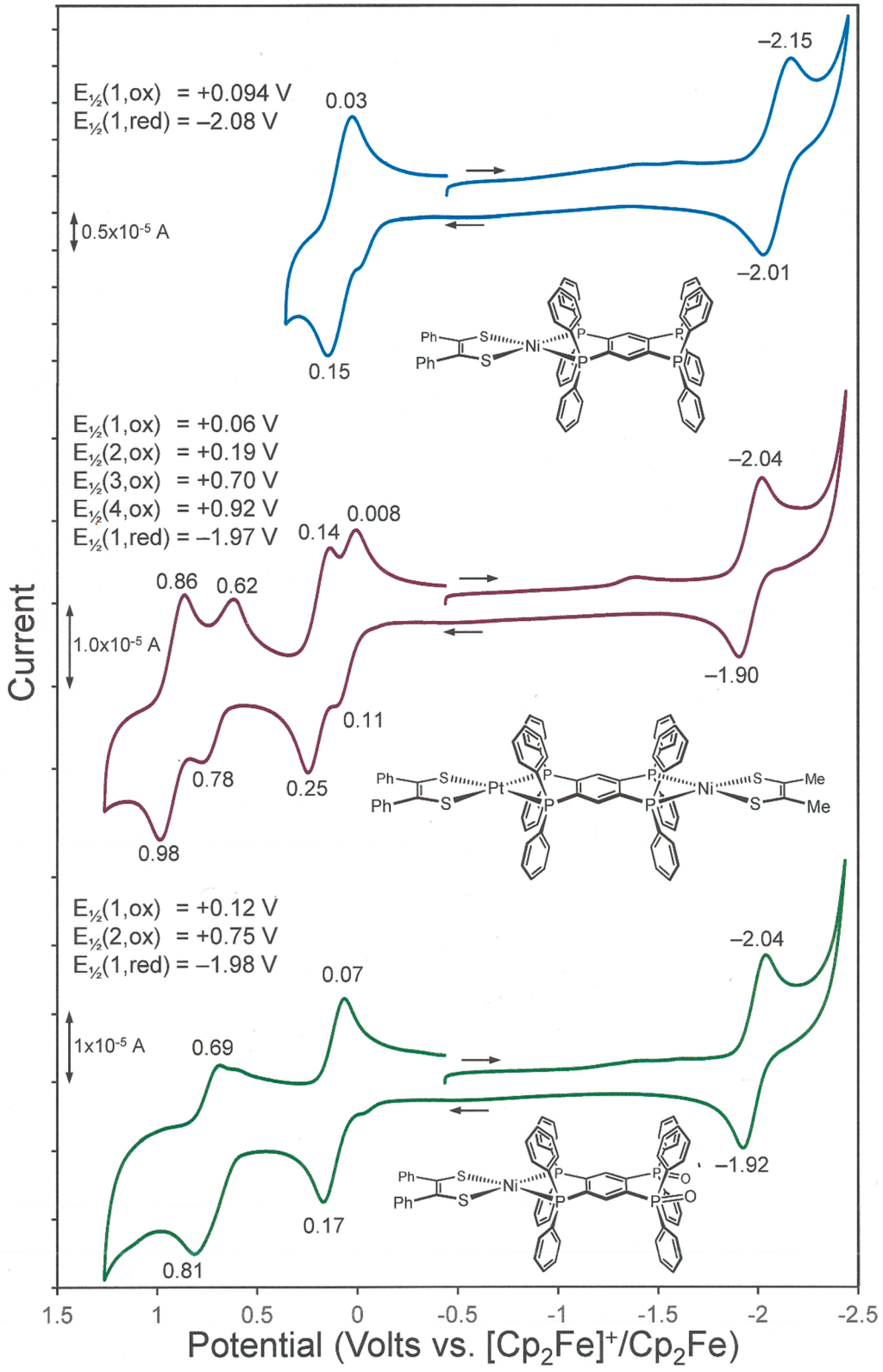

Figure 4. Cyclic voltammetry of selected compounds from Schemes 2 and 3.

compounds, it is unclear why reversible behavior is not sustained under the same conditions. The cathodic direction reveals a single $1e^-$ reduction for $[(R_2C_2S_2)M(tpbz)]$ that is due to a reduction of the tpbz ligand. The more comparable scaling of the current amplitude for this reduction relative to the oxidation waves is consistent with the assignment of all processes as one-electron events (Figure 4 (top)). In contrast, the oxidation waves in $[(R_2C_2S_2)M(tpbz)M(S_2C_2R_2)]$ are $2e^-$ processes and display substantially greater current compared to the reduction wave, which is also due to the reduction of tpbz.

https://doi.org/10.1021/acs.inorgchem.1c01573
Inorg. Chem. 2021, 60, 13177–13192

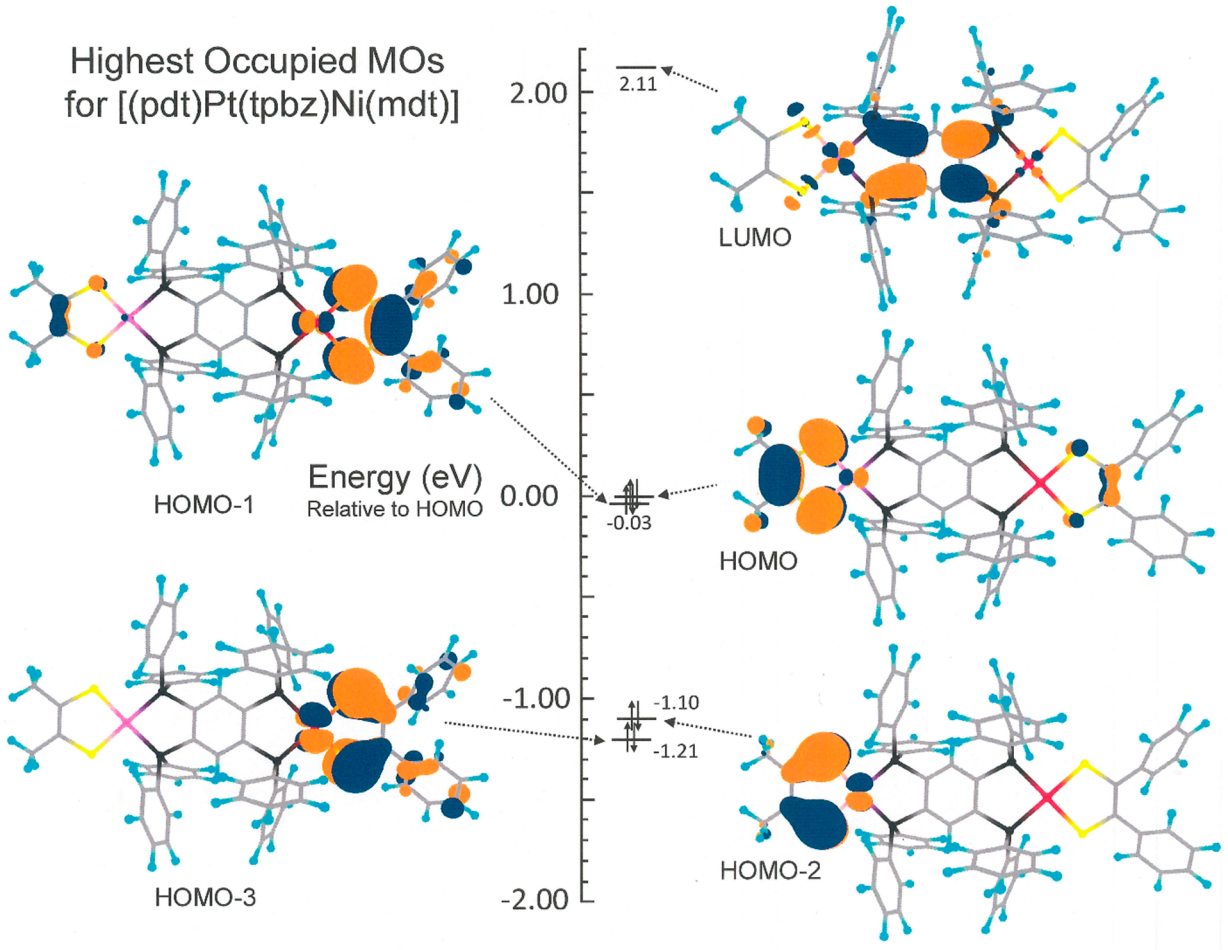

Figure 5. Frontier molecular orbitals for $[(Ph_2C_2S_2)Pt(tpbz)Ni(S_2C_2Me_2)]$, showing the HOMO and HOMO−1 to be largely localized at the $Ni(S_2C_2Me_2)$ and $Pt(S_2C_2Ph_2)$ ends, respectively. Orbital images are shown at the 0.03 contour level.

In open-ended $[(R_2C_2S_2)M(tpbz)]$, the reduction wave is shifted to a more negative potential than that in the corresponding dimetallic compound. Here again, the effect is accounted for by the greater electron richness of the tpbz ligand when metalated at one end instead of both. The description of these redox events is corroborated by structure optimizations that reveal the HOMO and LUMO for **8** to be dithiolene-based and predominantly tpbz-based, respectively (Figure S116).

Because of the asymmetry in **15**, the successive oxidation waves that arise from ene-1,2-dithiolate to radical monoanion (Scheme 1, **a** → **b**) and radical monoanion to α-dithione (Scheme 1, **b** → **c**) oxidation are partially resolved [Figure 4 (middle)]. In our earlier study involving the centrosymmetric homodimetallic compounds $[(R_2C_2S_2)M(tpbz)M(S_2C_2R_2)]$,[2] a consistent anodic shift of +0.04−0.05 V was observed upon moving from the methyl- to phenyl-substituted dithiolene ligand, while the metal ion was constant as either Ni^{2+}, Pd^{2+}, or Pt^{2+}. This difference was attributed to a modestly greater electron-donating effect for Me over Ph, which enables the ligand-based oxidation to occur at a less positive potential. Similarly, the change in $[(R_2C_2S_2)M(tpbz)M(S_2C_2R_2)]$ from Ni^{2+} to Pt^{2+} with a constant dithiolene ligand occasioned a +0.13−0.14 V anodic shift, which was ascribed to a greater dipositive character of the third-row metal compared to the first-row metal. Assuming the effects of the dithiolene substituent and of the metal-ion identity to be simply additive leads to the prediction that $[(Ph_2C_2S_2)Pt(tpbz)Ni(S_2C_2Me_2)]$ would undergo oxidation at its $Ni(S_2C_2Me_2)$ end first, with ∼0.18 V separating that process from an oxidation of the same nature at the $Pt(S_2C_2Ph_2)$ end. As gauged by the anodic and cathodic maxima in the voltammogram [Figure 4 (middle)], the $\Delta E_{1/2}$ separating the first and second oxidation processes is ∼0.13 V, while the $\Delta E_{1/2}$ between the third and fourth waves is ∼0.22 V. The assignment of the first anodic wave as $Ni(^{-}S_2C_2Me_2) - 1e^{-} \rightarrow Ni(^{-}S^{\bullet}SC_2Me_2)^{+}$ and the second as $(Ph_2C_2S^{-}{}_2)Pt - 1e^{-} \rightarrow (Ph_2C_2S^{-}S^{\bullet})Pt^{+}$ is affirmed by a geometry optimization of **15**. The calculated electronic structure shows the HOMO to be predominantly constituted of the $Ni(S_2C_2Me_2)$ end, while the HOMO−1, which likely becomes the HOMO in $[\mathbf{15}]^{+}$, is largely localized at the opposite $(Ph_2C_2S_2)Pt$ terminus (Figure 5). The $1e^{-}$ cathodic wave at −1.97 V, which arises from a reduction of the tpbz ligand, occurs at a potential very similar to its place in the homodimetallic compounds.

Although they have been known for some time,[8,21,29−31] platinum dithiolene compounds of the type $[(R_2C_2S_2)_2Pt(phosphine)_2]$ have been little studied electrochemically. In the oxidizing direction, the cyclic voltammogram of **10** reveals multiple reversible and partially reversible waves (Figure S75). Given the reduced state of the dithiolene ligand, as inferred from the structural data, these processes are likely successive $1e^{-}$ oxidations of the dithiolene ligands, of which there are four in principle. Cathodic scanning reveals irreversible behavior

https://doi.org/10.1021/acs.inorgchem.1c01573
Inorg. Chem. 2021, 60, 13177−13192

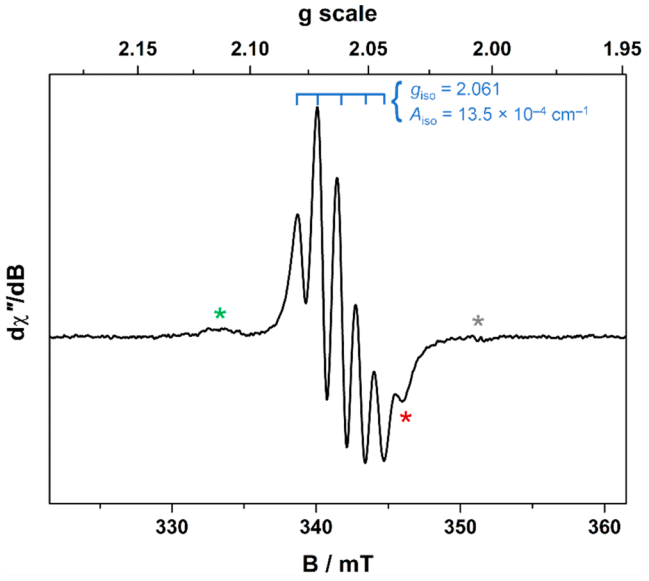

Figure 6. X-band EPR spectrum of **8** treated with 2 equiv of tris(4-bromophenyl)ammoniumyl hexachloroantimonate in CH_2Cl_2 recorded at room temperature (experimental conditions: frequency, 9.8587 GHz; power, 6.3 mW; modulation, 0.4 mT). The main signal indicated in blue comprises the five lines with g_{iso} = 2.061 and A_{iso} = 13.5 × 10^{-4} cm^{-1}. Minor signals are denoted with the red and green asterisks. The gray asterisk references the position of the oxidant ($g \sim$ 2.0036).

beginning at ~−1.22 V versus the $[Cp_2Fe]^+/[Cp_2Fe]$ couple, which is likely metal-based and possibly leads to the extrusion of one of the dithiolene ligands.

EPR Spectroscopy. An aliquot of **8** was treated with successive equivalents of tris(4-bromophenyl)ammoniumyl hexachloroantimonate and monitored by EPR spectroscopy. The addition of 0.5 and 1 equiv of oxidant yielded no signal, although the reduction potential of the oxidant 0.7 V (vs $Fc^{+/0}$) is sufficient to oxidize this compound.[32] At >1 equiv, the main signal shown in the spectrum in Figure 6 appeared, which is comprised of fives lines in a binomial intensity pattern brought about by the coupling of four ^{31}P nuclei. The signal is short-lived, diminishing over the course of 2−3 h even in a Teflon-stoppered EPR tube. On the basis of its relative intensity and position, the feature denoted by the red asterisk is a separate signal, presumably the high-field hyperfine component of a multiline signal that lies beneath the main signal. A second minor signal is identified at $g \sim$ 2.011, as indicated by the green asterisk, and comprises a weakly resolved three-line binomial pattern.

At this stage, no definitive assignment can be made of the EPR signal. The g and A values are distinct from other paramagnetic nickel diphosphine species. For example, the spin doublet $[(adt^{\bullet})Ni^{II}(dppb)]^+$ has a three-line spectrum with g_{iso} = 2.0106 and A_{iso} = 3.3 × 10^{-4} cm^{-1}, while the spin triplet $[(adt^{\bullet})Ni^{II}(tpbz)Ni^{II}(adt^{\bullet})]^+$ has a five-line signal with g_{iso} = 2.011 and A_{iso} = 1.7 × 10^{-4} cm^{-1} [where adt^{2-} = bis(*p*-anisyl)-1,2-ethenedithiolate].[33] The hyperfine coupling constant is 25% of that in the spectrum in Figure 6. The g values are also noticeably smaller, where the higher value here is better matched by $[Ni(adt)(adt^{\bullet})]^-$ with g_{iso} = 2.0059 (but with no hyperfine splitting). In contrast, Ni-centered $S = {}^1/_2$ complexes with phosphine ligands have even larger hyperfine coupling constants, e.g., $[Ni^I(dppe)_2]^+$ with g_{iso} = 2.090 and A_{iso} = 83 × 10^{-4} cm^{-1} and $[(Et_2dtc)Ni^I(dppe)]^0$ with g_{iso} = 2.089 and A_{iso} = 81 × 10^{-4} cm^{-1} [dppe = 1,2-bis(diphenylphosphino)ethane; Et_2dtc = *N*,*N*-diethyldithiocarbamate].[30] The main signal here is consistent with four P donor atoms at a Ni^{II} center with a coordinated dithiolene radical and results from subsequent oxidation of the first oxidation product of the monometallic [(pdt)Ni(tpbz)]. The exact composition and construct of this paramagnetic species are not known at this time.

SUMMARY AND CONCLUSIONS

The principal findings of this work are the follows:

(1) Open-ended compounds of the type $[(R_2C_2S_2)M(tpbz)]$ can be prepared in good yields either by the direct reaction between charge-neutral $[(R_2C_2S_2)_2M]$ (M = Ni^{2+}, Pd^{2+}, Pt^{2+}; R = Me, Ph, *p*-anisyl) and tpbz or by transmetalation between $[Cl_2M(tpbz)]$ and $[(R_2C_2S_2)SnR'_2]$ (R = Me, R′ = ^{n}Bu; R = CN, R′ = Me).

(2) The open-ended $[(R_2C_2S_2)M(tpbz)]$ compounds reveal ^{31}P NMR signals in the 55−40 ppm range and at ~−15.0 ppm, corresponding respectively to the metalated and open ends, in clear distinction from their symmetric homodimetallic counterparts.

(3) The open-ended compounds are subject to the reaction types typical of chelating diphosphines. They may be oxidized to diphosphine dicalcogenides at their open end, and they may be metalated asymmetrically with an altogether different ML_n fragment.

(4) The cyclic voltammogram of the asymmetric heterodimetallic compound $[(Ph_2C_2S_2)Pt(tpbz)Ni(S_2C_2Me_2)]$ shows two pairs of closely spaced, but resolved, 1e$^-$ oxidations that correspond to the successive oxidation of each metallodithiolene end group, first to the radical monoanion state and then to the α-dithione. In contrast, the centrosymmetric homodimetallic $[(R_2C_2S_2)M(tpbz)M(S_2C_2R_2)]$ compounds show two 2e$^-$ oxidation waves.

In forthcoming reports, we detail the syntheses, structures, and properties of heterotrimetallic compounds of the form $[[(R_2C_2S_2)M(\mu\text{-tpbz})]_2M'L_x]^n$, where $M'L_x$ is a either a charge-neutral fragment or a cation, using the monometallic $[(R_2C_2S_2)M(tpbz)]$ complexes described here as fungible building units.

ASSOCIATED CONTENT

Supporting Information

The Supporting Information is available free of charge at https://pubs.acs.org/doi/10.1021/acs.inorgchem.1c01573.

Procedures for crystal growth, X-ray diffraction data collection, and structure solution and refinement, summaries of the unit cell and refinement data (Tables S1−S4), thermal ellipsoid plots with complete atom labeling (Figures S1−S23), spectroscopic, electrochemical, and analytical data for the compounds reported (Figures S24−S115), a description of the computational procedures, an MO energy level diagram for **8** (Figure S116), and coordinates for geometry-optimized **15** and **8** (Tables S6 and S7) (PDF)

Accession Codes

CCDC 2024446−2024456 and 2076132−2076135 contain the supplementary crystallographic data for this paper. These data can be obtained free of charge via www.ccdc.cam.ac.uk/data_request/cif, or by emailing data_request@ccdc.cam.ac.uk, or by contacting The Cambridge Crystallographic Data

https://doi.org/10.1021/acs.inorgchem.1c01573
Inorg. Chem. 2021, 60, 13177−13192

Centre, 12 Union Road, Cambridge CB2 1EZ, UK; fax: +44 1223 336033.

AUTHOR INFORMATION

Corresponding Authors

Satyendra Kumar − *Department of Chemistry, Tulane University, New Orleans, Louisiana 70118, United States;* Present Address: Xavier University of Louisiana, 1 Drexel Drive, New Orleans, Louisiana 70125; Email: skumar5@tulane.edu

James P. Donahue − *Department of Chemistry, Tulane University, New Orleans, Louisiana 70118, United States;* orcid.org/0000-0001-9768-4813; Email: donahue@tulane.edu

Authors

Malathy Selvachandran − *Department of Chemistry, Tulane University, New Orleans, Louisiana 70118, United States;* Present Address: University of Jaffna, Vavuniya Campus, Jaffna, Sri Lanka.

Kuppuswamy Arumugam − *Department of Chemistry, Wright State University, Dayton, Ohio 45435-0001, United States;* orcid.org/0000-0003-2654-5001

Mohamed C. Shaw − *Department of Chemistry, Tulane University, New Orleans, Louisiana 70118, United States*

Che Wu − *Department of Chemistry, Tulane University, New Orleans, Louisiana 70118, United States*

Michael Maurer − *Department of Chemistry, Tulane University, New Orleans, Louisiana 70118, United States*

Xiaodong Zhang − *Department of Chemistry, Tulane University, New Orleans, Louisiana 70118, United States*

Stephen Sproules − *WestCHEM, School of Chemistry, University of Glasgow, Glasgow G12 8QQ, United Kingdom;* orcid.org/0000-0003-3587-0375

Joel T. Mague − *Department of Chemistry, Tulane University, New Orleans, Louisiana 70118, United States*

Complete contact information is available at: https://pubs.acs.org/10.1021/acs.inorgchem.1c01573

Notes

The authors declare no competing financial interest.

ACKNOWLEDGMENTS

The Louisiana Board of Regents [Grant LEQSF-(2002-03)-ENH-TR-67] and the National Science Foundation (Grant MRI 1228232 and 0619770) are thanked for funding of Tulane University's X-ray crystallography and mass spectrometry instrumentation, and Tulane University is acknowledged for its ongoing assistance with operational costs for the X-ray diffraction facility. S.K. and J.P.D. gratefully acknowledge support for this project from the National Science Foundation (Grant CHE 1836569).

REFERENCES

(1) Arumugam, K.; Shaw, M. C.; Mague, J. T.; Bill, E.; Sproules, S.; Donahue, J. P. Long Range Spin Coupling: A Tetraphosphine-Bridged Palladium Dimer. *Inorg. Chem.* **2011**, *50*, 2995−3002.

(2) Arumugam, K.; Selvachandran, M.; Obanda, A.; Shaw, M. C.; Chandrasekaran, P.; Caston Good, S. L.; Mague, J. T.; Sproules, S.; Donahue, J. P. Redox-Active Metallodithiolene Groups Separated by Insulating Tetraphosphinobenzene Spacers. *Inorg. Chem.* **2018**, *57*, 4023−4038.

(3) Zahavy, E.; Fox, M. A. An Os^{II}-Ni^{II}-Pd^{II} Trimetallic Complex as an Electro-Switchable-Photoinduced-Electron-Transfer Device. *Chem. - Eur. J.* **1998**, *4*, 1647−1652.

(4) Chen, T.-H.; Popov, I.; Kaveevivitchai, W.; Miljanić, O. Š. Metal-Organic Frameworks: Rise of the Ligands. *Chem. Mater.* **2014**, *26*, 4322−4325.

(5) Eisenhart, R. J.; Clouston, L. J.; Lu, C. C. Configuring Bonds between First-Row Transition Metals. *Acc. Chem. Res.* **2015**, *48*, 2885−2894.

(6) Boudier, A.; Breuil, P.-A. R.; Magna, L.; Olivier-Bourbigou, H.; Braunstein, P. Nickel(II) Complexes with Imino-Imidazole Chelating Ligands Bearing Pendant Donor Groups (SR, OR, NR_2, PR_2) as Precatalysts in Ethylene Oligomerization. *J. Organomet. Chem.* **2012**, *718*, 31−37.

(7) Hartley, F. R.; Murray, S. G.; McAuliffe, C. A. Monomeric Complexes of Palladium(II) and Platinum(II) with a Series of Open-Chain Tetrathioether Ligands Prepared from Complexes of Weak Donor Ligands. *Inorg. Chem.* **1979**, *18*, 1394−1397.

(8) Schrauzer, G. N.; Mayweg, V. P. Preparation, Reactions, and Structure of Bisdithio-α-diketone Complexes of Nickel, Palladium and Platinum. *J. Am. Chem. Soc.* **1965**, *87*, 1483−1489.

(9) McFarlane, H. C. E.; McFarlane, W. Polyphosphorus Ligands − V.* The Synthesis, Phosphorus-31 NMR Spectra and Conformations of the Polykis(diphenylphosphino) Benzenes $(Ph_2P)_nC_6H_{6-n}$ (n = 1−4). *Polyhedron* **1988**, *7*, 1875−1879.

(10) Genge, A R. J.; Levason, W.; Reid, G. Multinuclear NMR Studies of Diphosphine, Diphosphine-Dioxide and Diarsine Complexes of Tin(IV) Halides. Structures of $[SnI_4\{o\text{-}C_6H_4(AsMe_2)_2\}]$ and $[SnI_4\{o\text{-}C_6H_4(P(O)Ph_2)_2\}]$. *Inorg. Chim. Acta* **1999**, *288*, 142−149.

(11) Armarego, W. L. F.; Perrin, D. D. *Purification of Laboratory Chemicals*, 4th ed.; Butterworth-Heinemannn: Oxford, U.K., 2000.

(12) Arumugam, K.; Shaw, M. C.; Chandrasekaran, P.; Villagrán, D.; Gray, T. G.; Mague, J. T.; Donahue, J. P. Synthesis, Structures, and Properties of 1,2,4,5-Benzenetetrathiolate Linked Group 10 Metal Complexes. *Inorg. Chem.* **2009**, *48*, 10591−10607.

(13) Chandrasekaran, P.; Arumugam, K.; Jayarathne, U.; Pérez, L. M.; Mague, J. T.; Donahue, J. P. Synthesis, Structures, and Properties of Mixed Dithiolene-Carbonyl and Dithiolene-Phosphine Complexes of Tungsten. *Inorg. Chem.* **2009**, *48*, 2103−2113.

(14) Usón, R.; Vicente, J.; Oro, J. Maleonitriledithiolate Complexes of Au(III), Au(I), Pd(II), and Pt(II) Containing Neutral or Anionic Ligands. *Inorg. Chim. Acta* **1981**, *52*, 29−34.

(15) Cerrada, E.; Fernández, E. J.; Gimeno, M. C.; Laguna, A.; Laguna, M.; Terroba, R.; Villacampa, M. D. Synthesis of Dithiolate Gold(III) Complexes by Dithiolate Transfer Reactions. X-ray Structure of $[Au(C_6F_5)(S_2C_6H_4)(PPh_3)]$. *J. Organomet. Chem.* **1995**, *492*, 105−110.

(16) Cerrada, E.; Fernández, E. J.; Jones, P. G.; Laguna, A.; Laguna, M.; Terroba, R. Synthesis and Reactivity of Trinuclear Gold(III) Dithiolate Complexes. X-Ray Structure of $[Au(C_6F_5)(S_2C_6H_4)]_3$ and $[Au(C_6F_5)(S_2C_6H_4)(SC_6H_4SPPh_3)]$. *Organometallics* **1995**, *14*, 5537−5543.

(17) Nomura, M.; Fourmigué, M. Dinuclear Cp* Cobalt Complexes of the 1,2,4,5-Benzenetetrathiolate Bischelating Ligand. *Inorg. Chem.* **2008**, *47*, 1301−1312.

(18) McGuire, J.; Miras, H. N.; Richards, E.; Sproules, S. Enabling Single Qubit Addressability in a Molecular Semiconductor Comprising Gold-Supported Organic Radicals. *Chem. Sci.* **2019**, *10*, 1483−1491.

(19) Shimizu, T.; Murakami, H.; Kobayashi, Y.; Iwata, K.; Kamigata, N. Synthesis, Structure, and Ring Conversion of 1,2-Dithiete and Related Compounds. *J. Org. Chem.* **1998**, *63*, 8192−8199.

(20) Obanda, A.; Martinez, K.; Schmehl, R. H.; Mague, J. T.; Rubtsov, I. V.; MacMillan, S. N.; Lancaster, K. M.; Sproules, S.; Donahue, J. P. Expanding the Scope of Ligand Substitution from $[(Ph_2C_2S_2)_2M]$ (M = Ni^{2+}, Pd^{2+}, Pt^{2+}) to Afford New Heteroleptic Dithiolene Complexes. *Inorg. Chem.* **2017**, *56*, 10257−10267.

(21) Chandrasekaran, P.; Greene, A. F.; Lillich, K.; Capone, S.; Mague, J. T.; DeBeer, S.; Donahue, J. P. A Structural and

Spectroscopic Investigation of Octahedral Platinum Bis(dithiolene)-phosphine Complexes: Platinum Dithiolene Internal Redox Chemistry Induced by Phosphine Association. *Inorg. Chem.* **2014**, *53*, 9192−9205.
(22) Connick, W. B.; Gray, H. B. Photooxidation of Platinum(II) Diimine Dithiolates. *J. Am. Chem. Soc.* **1997**, *119*, 11620−11627.
(23) Brock, C. P.; Schweizer, W. B.; Dunitz, J. D. Internal Molecular Motion of Triphenylphosphine Oxide: Analysis of Atomic Displacement Parameters for Orthorhombic and Monoclinic Crystal Modifications at 100 and 150 K. *J. Am. Chem. Soc.* **1985**, *107*, 6964−6970.
(24) Davis, M. F.; Levason, W.; Reid, G.; Webster, M. Synthesis and Characterization of Tin(IV) Fluoride Complexes of Phosphine and Arsine Oxide Ligands. *Polyhedron* **2006**, *25*, 930−936.
(25) Codding, P. W.; Kerr, K. A. Triphenylphosphine Sulfide. *Acta Crystallogr., Sect. B* **1978**, *34*, 3785−3787.
(26) Clegg, W.; Edwards, A. J.; McFarlane, H. C. E.; McFarlane, W. 1,2,3,5-Tetrakis(diphenylthiophosphino)benzene: N.M.R. and X-ray Diffraction Studies of a Markedly Distorted Aromatic Molecule. *Polyhedron* **1998**, *17*, 3515−3518.
(27) Hursthouse, M. B.; Levason, W.; Ratnani, R.; Reid, G.; Stainer, H.; Webster, M. Synthesis, Spectroscopic and Structural Properties of an Unusual Series of Homoleptic Phosphine Oxide Complexes of the Alkaline Earth Dications. *Polyhedron* **2005**, *24*, 121−128.
(28) Schwab, M. M.; Himmel, D.; Kacprzak, S.; Radtke, V.; Kratzert, D.; Weis, P.; Wernet, M.; Peter, A.; Yassine, Z.; Schmitz, D.; Scheidt, E.-W.; Scherer, W.; Weber, S.; Feuerstein, W.; Breher, F.; Higelin, A.; Krossing, I. Synthesis, Characterizations, and Reactions of Truly Cationic Ni^{I}−Phosphine Complexes. *Chem. - Eur. J.* **2018**, *24*, 918−927.
(29) Mayweg, V. P.; Schrauzer, G. N. Bis-adducts of Group VIII Metal Bisdithiobenzil Complexes with Phosphines. *Chem. Commun.* **1966**, 640−641.
(30) Bowmaker, G. A.; Boyd, P. D. W.; Campbell, G. K. Electrochemical and ESR Studies of the Redox Reactions of Nickel(II), Palladium(II), and Platinum(II) Complexes of 1,2-Diphenyl-1,2-ethenedithiolate(2−)-*S*,*S*'. *Inorg. Chem.* **1983**, *22*, 1208−1213.
(31) Nomura, M.; Okuyama, R.; Fujita-Takayama, C.; Kajitani, M. New Synthetic Methods for η^5-Cyclopentadienyl Nickel(III) Dithiolene Complexes Derived from Nickelocene. *Organometallics* **2005**, *24*, 5110−5115.
(32) Connelly, N. G.; Geiger, W. E. Chemical Redox Agents for Organometallic Chemistry. *Chem. Rev.* **1996**, *96*, 877−910.
(33) McGuire, J.; Miras, H. N.; Donahue, J. P.; Richards, E.; Sproules, S. Ligand Radicals as Modular Organic Electron Spin Qubits. *Chem. - Eur. J.* **2018**, *24*, 17598−17605.

https://doi.org/10.1021/acs.inorgchem.1c01573
Inorg. Chem. 2021, 60, 13177−13192